



Damping Techniques for Grid-Connected Voltage Source Converters based on LCL filter: An Overview

A. F. Cupertino, H. A. Pereira and C .C. Gomes

Publication:

Renewable and Sustainable Energy Reviews

DOI (*link to publication from Publisher*):

[10.1016/j.rser.2017.07.050](https://doi.org/10.1016/j.rser.2017.07.050)

Publication year:

2018

Document Version:

Accepted author manuscript, peer reviewed version

Citation for published version:

A. F. Cupertino, H. A. Pereira, and C . C .Gomes " Damping Techniques for Grid-Connected Voltage Source Converters based on LCL filter: An Overview," Renewable and Sustainable Energy Reviews, vol.81, no. 1, pp. 116-135, January 2018.

doi: [10.1016/j.rser.2017.07.050](https://doi.org/10.1016/j.rser.2017.07.050)

General rights

Copyright and moral rights for the publications made accessible in the public portal are retained by the authors and/or other copyright owners and it is a condition of accessing publications that users recognise and abide by the legal requirements associated with these rights.

- Users may download and print one copy of any publication from the public portal for the purpose of private study or research.
- You may not further distribute the material or use it for any profit-making activity or commercial gain
- You may freely distribute the URL identifying the publication in the public portal

Take down policy

If you believe that this document breaches copyright please contact us at gesepufv@gmail.com providing details, and we will remove access to the work immediately and investigate your claim.

Damping Techniques for Grid-Connected Voltage Source Converters based on LCL filter: An Overview

Camilo C. Gomes¹, Allan F. Cupertino^{2,3}, Heverton A. Pereira¹

¹ Department of Electrical Engineering, Federal University of Viçosa, Av. P. H. Rolfs s/n, 36570-900, Viçosa - MG, Brazil

² Graduate Program in Electrical Engineering, Federal University of Minas Gerais, Av. Antônio Carlos 6627, 31270-901, Belo Horizonte-MG, Brazil

³ Department of Materials Engineering, Federal Center for Technological Education of Minas Gerais, Av. Amazonas 5253, 30421-169, Belo Horizonte - MG, Brazil

camilo.coelho@ufv.br, allan.cupertino@yahoo.com.br, heverton.pereira@ufv.br

Abstract: Distributed generation systems have been expanded considerably in recent years. These systems are generally based on power electronics converters, whose switching harmonics need to be reduced by means of passive filters. LCL filter is a solution that has been strongly employed. However, LCL filter presents a resonant frequency that needs to be damped. This work presents a detailed review on the topics involving the mathematical modeling and design of the main structures and strategies for damping in a grid-connected three-phase PV system based on LCL filter. Four techniques are analyzed: Series passive damping (SPD), capacitor current feedback based strategy (CCF), capacitor voltage feedback based strategy (CVF) and notch filter based method (NF). This study analyzes low frequency models, control design and operation in weak grid conditions. Finally, transfer functions of the harmonic rejection capability of each damping strategy are illustrated. This work finishes with a case study of a 10 kW inverter, which evaluates all issues previously approached.

Keywords: Distributed generation systems, LCL filter, damping strategies, weak grid conditions, harmonic rejection analysis.

1. Introduction

Renewable energy sources have gained attention in recent years. Grid-connected solar photovoltaic systems are among these sources and play an important role in distributed generation [1]. Grid-connected systems can be installed close to loads, thus reducing line losses, improving the voltage profile and enhancing the reliability of the distribution system [2]. Nevertheless, photovoltaic panels generate direct voltage. Thus, power inverters are employed in order to inject the generated power into the electrical ac-grid [3].

One of the possible power inverter structure is presented in Fig. 1. This structure is a voltage source converter based on semiconductor switches, which are controlled by a modulation strategy. Consequently, the inverter switching generates harmonic voltages [4]. If these harmonics are not correctly filtered, harmonic currents can flow into the

power system [5]. In order to reduce harmonic currents flowing into the power systems, IEEE 519 recommendation and IEC 61000 standard define the level of harmonic currents that can be injected into the Point of Common Coupling (PCC) [6,7].

Thereby, passive filters are connected at the inverter output in order to mitigate the current harmonic content, as suggested in Fig. 1. Many topologies of passive filters are presented in literature, such as L filter [8], LC filter [9–13] and LCL filter [4,14–17]. Other topologies with larger number of elements and increased complexity have also been proposed [18–22].

Initially, pure inductive filters (L) were proposed in the literature, mainly due to its simplicity [23]. L topology is a first order filter, thus, a high-value inductor is generally necessary to attenuate the harmonics current, according to the standards. Large inductance values generate a high voltage drop and affect the control time response [5,23]. Therefore, higher switching frequencies need to be employed in order to reduce the passive elements. Nevertheless, the increased switching frequency raises losses in the power converter [23].

LC filter was proposed as an alternative to single L filter. The LC filter second order characteristic increases the attenuation for high frequencies and reduces filter volume [9–13]. The drawbacks of this topology are the existence of a resonance frequency, which can amplify high-orders current harmonic components, and the presence of inrush currents in the output capacitance [5,23].

LCL filter is a third order filter, which has recently gained attention as an alternative to LC filters and has been used in most voltage sources applications [14–16,24]. This topology results in volume and voltage drop reduction through the inductors, if compared with the L topology [25]. Furthermore, the second inductance limits the capacitor inrush current and increases the inverter robustness due to grid inductance variations [4,14]. The complexity of the system (third order) and the resonance frequency are drawbacks of this topology [5].

More complex topologies are proposed in literature [18–22]. These topologies result in a frequency response with a lager attenuation at the switching frequency based on traps with series resonances. In the LLCL filter topology, for example, a small inductor is inserted in the branch loop of the capacitor in the traditional LCL filter to compose a series resonant circuit at the switching frequency [19]. This filter topology can attenuate the switching-frequency current ripple components much better than an LCL filter, leading to a decrease in the total inductance and volume. However, this filter attenuates less than the LCL filter above the twice times of switching frequency [5,18]. Other possible implementations are recently discussed by [26].

Nevertheless, the complexity of the control system increases significantly and the dynamic performance of the inverter can also be affected when more complex filter structures are employed. Therefore, these topologies are interesting in the field of high power applications, which employ low switching frequencies [22]. In this case, the same attenuation can be reached with smaller components, reducing the weight and volume, once these variables are critical in high power converters. Other possible approach is combine the LCL filter design with a proper modulation strategy with selective harmonic elimination (SHE), as proposed by [27].

In grid-connected applications with LCL filters, the current is generally controlled in synchronism with the PCC voltage [1,4,15]. In this situation, it is possible to control the active and reactive power injected into the grid [1,28]. The controller design is generally based on a low frequency model of LCL filter [15]. However, LCL filter presents a

resonance frequency which may cause instability in the closed loop system [29–31]. This problem is reported in many works in the literature and many damping methods are proposed to solve it [5,14,30,32].

Damping methods can be sorted into two groups: passive and active damping. Passive damping consists in inserting passive elements in the filter, in order to reduce the resonant peak of the system [30]. In general, passive damping techniques do not require any modification in the control strategy. However, these methods change filter attenuation and increase losses [17,30,33]. A passive damping technique presented in many works in the literature consists in adding a simple resistor in series with the filter capacitor [4,14]. As drawbacks, this technique reduces filter attenuation, increasing in the power losses and filter volume [5].

In order to solve the drawbacks associated to passive damping methods, active damping methods have been proposed. Active damping methods consist in modifications in the control strategy in order to provide closed loop damping [34]. Reference [5] proposes the classification of active damping techniques into 3 groups: single loop methods, multi-loop methods and complex controllers based methods.

Single loop methods are applied to damp the LCL filter resonance, without additional measurement. These methods include: low pass filter based method [24], virtual flux estimation based method [35], sensorless method [36], splitting capacitor-LCCL based method [37], notch-filter based method [16] and grid current feedback [38]. In general, single loop methods are little robust during parameters uncertainty and grid inductance variation [5]. Recently, a robust grid current feedback strategy based on a high-pass filter is proposed by [39].

Multiloop methods explore additional measurements. This group includes: capacitor current feedback [14,32,40,41], capacitor voltage feedback [4,14,15,32] and weighted average current control [42,43]. The robustness of these techniques for grid inductance variation tends to be improved compared with single loop techniques [5].

The last group of active damping methods are based on complex control structures. These techniques generally result in a satisfactory and robust dynamics. These methods include predictive control [44], adaptive controllers [45], vector control [46], sliding mode controller [47] and state-space controllers [3].

Furthermore, when LCL filter is chosen, there are two possibilities for current control: grid current (i_g) or converter current (i_f). According to [29], grid current control is more stable than converter current. This fact is also related in [48], where the grid current control resulted in a stable response even without any damping method. On the other hand, according to [31], the converter current presents an inherent damping that can result in larger stability if correctly explored. Therefore, there is an evident disagreement in literature about this issue and the selection of the current control strategy must be carefully analyzed.

Additionally, there are few publications in literature which compare the active damping techniques considering weak grid conditions. Distribution systems characterized by long distribution feeders and low-power transformers result in a power system with large impedance. Furthermore, according to [49], when converters with similar characteristics are connected in parallel, the equivalent grid inductance increases and its value is multiplied by the number of converters. Variations in the grid inductance affects the filter resonance frequency and can reduce current control stability [50]. Recently, reference [51] analyzes the resonance of multi-parallel inverters under an asynchronous carriers conditions. Additionally, reference [52] proposes a current separation scheme

which reveals that an interactive resonant current that circulates between the paralleled three-phase inverters may arise, depending the system resonance characteristics.

Reference [15] presents a LCL filter design methodology in order to provide stable operation under weak grid conditions. Passive damping, capacitor current feedback and capacitor voltage feedback techniques are approached. Nevertheless, this reference considers a grid with harmonic free condition, similarly to most works found in literature. The study on the harmonic rejection capability is an important issue under weak grid conditions, since distorted voltages can appear in the PCC [53].

In view of the points aforementioned, this work provides a detailed review on the topics involving the mathematical modeling and design of the main structures and strategies for damping in a grid-connected three-phase PV system based on LCL filter, as illustrated in Fig. 1. The objective is clarify to the readers the effect of the damping strategies in an analytical way. A review of the important details is discussed and, unfortunately, to include all damping strategies proposed in literature is not feasible. Therefore, four techniques mentioned are analyzed, once they are the most cited in literature: passive damping based on series resistor, capacitor current feedback based method, capacitor voltage feedback based method and notch-filter based method. The main issues approached in this review are:

- Mathematical modeling of damping techniques;
- Mathematical expressions of low frequency models for the approached techniques;
- Models for the harmonic rejection analysis, in order to evaluate the performance of each strategy towards grid voltage harmonic conditions.

The review finishes with a case study consisting in a three-phase photovoltaic inverter of 10 kW. Simulations are implemented in order to verify the dynamic behavior of each technique in time domain.

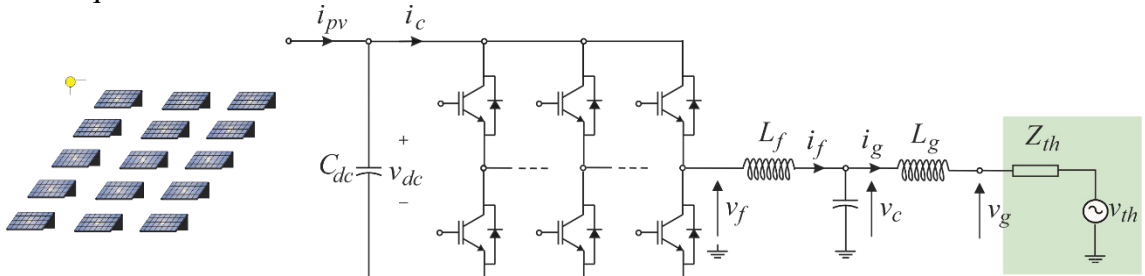


Fig. 1. Grid-connected photovoltaic inverter with output LCL filter.

This work is organized as follows. Section 2 presents a review on LCL filter design approaches and some limits of the filter parameters in order to obtain a suitable design methodology. This section finishes with a design example for a 10 kW inverter. Section 3 presents a review on DG inverter control strategies based on LCL filter. The PI controller design are described in details. Section 4 presents the mathematical modeling and design constraints for the 4 damping strategies which are described in this paper. Section 5 presents simulation results of exploring the dynamic behavior of the studied damping strategies. Dynamic performance and harmonic distortion are also analyzed in section 5. Section 6 presents the harmonic rejection performance of the proposed

techniques. This analysis is based on a transfer function model, considering an experimental voltage profile. Finally, section 7 presents the conclusions of this work.

2. LCL filter design

This section presents important considerations on LCL filter modeling and design. The main aspects of frequency response and parameter limits are discussed. Furthermore, recent mathematical results and design procedures are explored. Finally, an example of design is presented.

2.1. Modeling of the filter and design approaches

Fig. 1 presents a grid-connected inverter with LCL filter. In a first approach, the filter is considered ideal, once magnetic and electrical losses are neglected. The transfer functions of LCL filter are presented in Table I, where ω_{res} is the resonance frequency of the LCL filter, given by:

$$\omega_{res} = 2\pi f_{res} = \sqrt{\frac{L_f + L_g}{L_f L_g C_f}} = \sqrt{\frac{1}{C_f} \left(\frac{1}{L_f} + \frac{1}{L_g} \right)}, \quad (1)$$

and Z_{LC} is given by:

$$Z_{LC} = \sqrt{\frac{1}{L_g C_f}}. \quad (2)$$

Table I. Main transfer functions of LCL filter considering ideal elements.

		Output			
		$I_f(s)$	$I_g(s)$	$V_f(s)$	$I_c(s)$
Input	$I_f(s)$	1	$\frac{s^2 + Z_{LC}^2}{Z_{LC}^2}$	$\frac{1}{L_f s} \frac{s^2 + Z_{LC}^2}{s^2 + \omega_{res}^2}$	$\frac{s^2 + Z_{LC}^2}{s^2}$
	$I_g(s)$	$\frac{Z_{LC}^2}{s^2 + Z_{LC}^2}$	1	$\frac{1}{L_f s} \frac{Z_{LC}^2}{s^2 + \omega_{res}^2}$	$\frac{Z_{LC}^2}{s^2}$
	$V_f(s)$	$L_f s \frac{s^2 + \omega_{res}^2}{s^2 + Z_{LC}^2}$	$L_f s \frac{s^2 + \omega_{res}^2}{Z_{LC}^2}$	1	$L_f \frac{s^2 + \omega_{res}^2}{s}$
	$I_c(s)$	$\frac{s^2}{s^2 + Z_{LC}^2}$	$\frac{s^2}{Z_{LC}^2}$	$\frac{1}{L_f} \frac{s}{s^2 + \omega_{res}^2}$	1

According to the Table I of the paper, the following transfer functions are valid for LCL filter with ideal components:

$$G_{if}(s) = \frac{I_f(s)}{V_f(s)} = \frac{1}{L_f s} \frac{s^2 + Z_{LC}^2}{s^2 + \omega_{res}^2}, \quad (3)$$

$$G_{ig}(s) = \frac{I_g(s)}{V_f(s)} = \frac{1}{L_f s} \frac{Z_{LC}^2}{s^2 + \omega_{res}^2}. \quad (4)$$

Thereby, for inverter current (i_f) a resonant frequency, given by (1), and an anti-resonant frequency given by (2) are evident. It is easy to see that:

$$\omega_{res} = \sqrt{\frac{1}{C_f} \left(\frac{1}{L_f} + \frac{1}{L_g} \right)} > \sqrt{\frac{1}{C_f} \left(\frac{1}{L_g} \right)} = Z_{LC}. \quad (5)$$

Therefore, the anti-resonance happens in a frequency smaller than the resonant frequency. For instance, if equal inductors are employed, $\omega_{res} = \sqrt{2} Z_{LC}$. Based on this information, the transfer function $G_{if}(s)$ presents the following behavior:

- In low frequency range, the inductive effect is predominant and the transfer function attenuation is 20 dB/decade;
- In average frequency range, an anti-resonant and a resonant frequency are observed;
- After the resonant frequency, the filter returns to increase the attenuation in 20 dB/decade.

Furthermore, the transfer function $G_{ig}(s)$ presents the following behavior:

- In low frequency range, the inductive effect is predominant and the transfer function attenuation increases 20 dB/decade;
- In average frequency range, only a resonant frequency is observed;
- After the resonant frequency, the filter behaves as a third order system, increasing the attenuation to 60 dB/decade.

As expected, the resonance and attenuation of the LCL filter are function of the passive elements. Many works in literature present methodologies to design the LCL filter passive components [14,25,28,54,55]. The literature suggests some limits for the filter parameters, which are described below.

- *Filter capacitance*: the capacitance value is a compromise between power factor decrease and injected current harmonic distortion. The maximum suggested value for the filter capacitance is 5 % of the nominal power in order to avoid overrating the converter. Furthermore, the power factor at the grid terminals can also be a function of the position of the sensors in the power converter, as related in [28]. Therefore, reference [28] proposes a capacitor design related with sensor positions. In this situation, the capacitor is calculated to result in a unitary power factor at the grid terminals. However, this approach can result in large filter inductances [14]. An alternative solution is changing the reference current in order to obtain a unitary power factor at the grid terminals. This solution is approached in [31], where grid voltage and converter current are measured;
- *Filter inductance*: The inductor design is dependent on the power level and the application. In general, the total inductance value is limited to 0.1 pu in order to limit the voltage drop. Larger inductances will imply in larger dc bus voltages that will increase significantly the switching losses of the power

converter [28,56]. In low power applications, where LCL filters are integrated in the converter, filter volume is an important parameter, and smaller perceptual values are employed [54]. For higher power levels, the filter is not usually integrated in the converter. In this case, inductor saturation and grid current quality are important aspects of the design. Therefore, perceptual values until 0.1 pu are also employed [54].

- *Resonance frequency:* The resonant frequency should be in a range larger than the grid frequency and smaller than the switching frequency, in order to avoid resonance in lower and higher harmonic orders. Reference [54] suggests the allocation of the resonance frequency at a range between ten times the grid frequency and half the switching frequency.

In view of the aforementioned design constraints, reference [54] proposes a design methodology for LCL filter. Similarly to [28], the inductance L_f is determined for the maximum acceptable current ripple. The capacitance is determined only for the maximum admissible reactive power. Finally, the second inductance is determined for the desired harmonic current attenuation. The design is oriented by the resonance frequency, which needs to be allocated at the range suggested by [54]. The same approach is considered by [57], where delta and wye connections for the filter capacitances are explored. Delta connection in filter capacitances reduces by 3 times the required capacitance value. However, the capacitor voltages increase by a factor equal to $\sqrt{3}$.

Alternatively, a mathematical modeling of current ripple is proposed by [56] in order to determine optimized values for filter parameters in terms of energy storage. An iterative design methodology is used to minimize the filter storage energy, and consequently, the volume.

Reference [58] proposes a design method in order to meet grid code requirements with reduced losses for passive damping. On the other hand, a more complete loss model including electric and magnetic losses is proposed in [55]. Based on losses estimation, an algorithm is proposed to optimize filter losses and volume.

Reference [57] provides a systematic design methodology for LCL filter, presenting the state-space mathematical modeling approach. The state-space mathematical modeling considers practical cases of delta and wye connected capacitors. The effects on possible grounding alternatives are discussed. The state-space modeling of a current controlled inverter is also discussed in [59].

Recently, reference [60] proposes a design method where the resonance frequency of the LCL filter is higher than the Nyquist frequency, i.e., half of the system sampling frequency. In this case, a very cost-effective LCL filter design can be achieved for the grid-connected converters, whose dominant switching harmonics may appear at double the switching frequency as in unipolar-modulated three-level full-bridge converters.

An important point is that most references consider passive damping in design methodologies. However, the filter parameters have a crucial impact on the stability of active damping methods, mainly due to the resonance frequency value. Furthermore, a robust design for grid inductance variation is interesting if the converter is submitted to weak grid conditions.

Therefore, reference [14] proposes a LCL filter design methodology to obtain robust performance for passive and active damping towards weak grid conditions. The volume of the filter and magnetic losses are not approached. However, it presents interesting mathematical results for LCL filter parameters, which complements the limits proposed

in [54]. This approach is also discussed recently by [61]. According to this reference, four key points should be analyzed in order to obtain a robust design towards weak grid conditions:

- Ratio between switching and resonance frequency $r_f = f_s/f_{res}$;
- Ratio between grid and converter inductance $r_L = L_g/L_f$;
- Ratio between the per unit values of the LCL filter total inductance and capacitance $r_q = l_T/c_f$;
- Grid current THD.

The effect of these parameters is summarized in Table II.

Table II. Important aspects in the design methodology proposed by [14].

Parameter	Important aspects
r_f	<ul style="list-style-type: none"> • <i>Passive damping</i>: elevated $r_f = \frac{f_s}{f_{res}}$ are chosen in order to reduce losses; • <i>Active damping</i>: The resonance frequency needs to be visible for the digital control. Therefore, r_f has a crucial effect; • <i>Series passive damping</i>: f_{res} can be allocated in the halfway between f_{bw} and f_s. Under such conditions, the interference of resonance frequency in the current control loop is reduced. Therefore, $r_f \approx 4.5$ is employed; • <i>Capacitor current feedback strategy</i>: The required ratio is $r_f \approx 3$. This value guarantees that the delay caused by digital implementation has no significant impact on system response close to the resonance frequency; • <i>Capacitor voltage feedback strategy</i>: The required ratio is $r_f \approx 3.2 - 3.4$. This value guarantees that the lead-lag network used in this active damping method approximates to an ideal differentiator.
r_L	<ul style="list-style-type: none"> • Affects the filter attenuation and the robustness towards grid impedance variations; • $r_L = 1$ implies in the minimum inductance values and minimum voltage drop across the filter. Additionally, this value also results in minimal capacitor C_f and consequently, minimum reactive power. Finally, equal inductors present economic advantages; • $r_L = 1$ results in the minimum attenuation. However, considering the range $0.5 < r_L < 2$, the attenuation increases only 12 %; • Increased r_L improves the robustness of the filter towards grid inductance variations, since the per unit resonance frequency variation decreases.
r_q	<ul style="list-style-type: none"> • The ratio between the filter inductance and capacitance has an impact on the reactive power and therefore on the filter power factor; • $r_q = 1$ nulls the filter reactive power and therefore, implies in any converter overrating; • $r_q = 1$ also corresponds to the minimum storage energy in the filter. Nevertheless, this definition results in large values of inductance and small values of filter capacitance; • Generally, r_q is increased, thus reducing the power factor at an acceptable range, providing acceptable values of inductance.
THD	<ul style="list-style-type: none"> • Increased r_f strongly reduces the grid current THD. This fact is observed because, when r_f is large, the switching frequency is allocated at a range in which filter attenuation is 60 dB/decade; • Increased r_L decreases the current THD due to the larger attenuation; • Increased r_q tends to increase the current THD.

2.2. Design limits

In view of the aspects aforementioned, this work suggests some mathematical limits which may help in a LCL filter design procedure. Nevertheless, the analysis of this work does not include limitations related to inductor volume and total losses.

The first guideline is related to the filter total reactive power. The converter overrating due to the filter reactive power needs to be smaller than 0.5 %. Under such conditions, the minimum power factor admissible for the filter is:

$$PF_{min} = \frac{1}{1.005} = 0.995. \quad (6)$$

This guideline contributes to limit the reactive power and the size of the filter capacitance. Actually, this limit is more restrictive than the 5 % of reactive power suggested by [54].

Additionally, the grid current total harmonic distortion needs to be smaller than 5 %. However, the estimate presented in section 2.5 is optimistic, since dead time effects, grid voltage harmonic distortion, dc bus voltage ripple and nonlinearities are neglected. Therefore, a security margin needs to be included. Thereby, a maximum value of 3 % is adopted for purposes of design.

The inductance is limited by 3 factors. Firstly, the total inductance needs to be smaller than 0.1 pu in order to limit the voltage drop. Under these conditions,

$$L_{max,\Delta V} = \frac{L_b}{10}. \quad (7)$$

where $L_b = \frac{Z_b}{\omega_n}$ and $Z_b = \frac{V_n^2}{S_n}$. V_n is the nominal voltage and S_n is the apparent power of the converter.

Additionally, the total filter inductance should be smaller than purely inductive filter. In fact, LCL filter is economic advantageous if its total inductance is smaller than an L filter. The design of a purely inductive filter is derived in [17]. Considering the maximum value of the grid current THD equal to 3 %, a superior limit for the LCL filter total inductance is given by:

$$L_{max,L} = \frac{100}{6\sqrt{3}} \frac{1}{\sqrt{48 f_s I_n}} \frac{V_{dc}}{\sqrt{f(m)}}, \quad (8)$$

where f_s is the switching frequency, V_{dc} is the dc-link voltage, I_n is the rated current and $f(m)$ is given by:

$$f(m) = \frac{3}{2}m^2 - \frac{4\sqrt{3}}{\pi}m^3 + \frac{9}{8}\left(\frac{3}{2} - \frac{9\sqrt{3}}{8\pi}\right)m^4. \quad (9)$$

m is the modulation index of fundamental component. This variable can be estimated by:

$$m = \frac{2\sqrt{2}}{V_{dc}} \sqrt{\left(\frac{V_n}{\sqrt{3}}\right)^2 + (2\pi f_n L_T I_n)^2}. \quad (10)$$

The last limit for the filter inductance is related with the current ripple in the first inductor. In fact, the maximum current ripple in the first inductor needs to be limited due to the power losses and heating. A value between 30 and 50% is used in some works in literature [28,54,56]. According to [56], the minimum inductance for reaching this criteria is given by:

$$L_{f,min} = \frac{V_g}{2\sqrt{6}f_s\Delta i_f}, \quad (11)$$

where V_g is the phase voltage and Δi_f is the current ripple in amperes.

This way, a lower limit for the converter total inductance, considering 30 % of current ripple, is given by:

$$L_{min} = (1 + r_L) \frac{5V_g}{3\sqrt{6}f_s I_n}. \quad (12)$$

In this situation, the filter total inductance is limited in the range:

$$L_{min} \leq L_T \leq L_{max}, \quad (13)$$

where $L_{max} = \min(L_{max,L}, L_{max,\Delta V})$.

The inductance value is generally chosen as close as possible to the minimum limit, which results in the minimum voltage drop at the filter terminals.

2.3. Design example

In this section, an example for LCL filter design is considered. The parameters of the photovoltaic inverter are presented in Table III.

Table III. Parameters of the photovoltaic inverter.

Parameter	Symbol	Value
Nominal apparent power	S_n	10 kVA
Grid voltage (line to line)	V_n	380 V
Line frequency	f_n	60 Hz
Switching frequency	f_s	6 kHz
Sampling frequency	f_{sp}	6 kHz
Dc bus voltage	V_{dc}	650 V

Firstly, the value of ratio r_f needs to be defined according to the damping strategy. In this example, it will be considered a passive damping strategy with $r_f = 3.3$. Therefore, the resonance frequency is $f_{res} \approx 1.82$ kHz. Furthermore, $r_L = 1$ is used to obtain equal inductors and minimum voltage drop.

Then, the filter total inductance L_T , the power factor PF and the grid current THD are plotted as function of r_q , as illustrated in Fig. 2. The mathematical relations of these variables can be found in [14]. Fig. 2 also illustrates the limits suggested for this work. Note that the total inductance should range between 2 and 4 mH. In this case, the selection of $r_q = 1.5$ results in the dots highlighted in the graphic. This choice results in the minimum voltage drop at the filter terminals added to an acceptable converter overrating and grid current THD. The parameters of the LCL filter considering this ratio are presented in Table IV. These parameters are used in all case studies presented in this work.

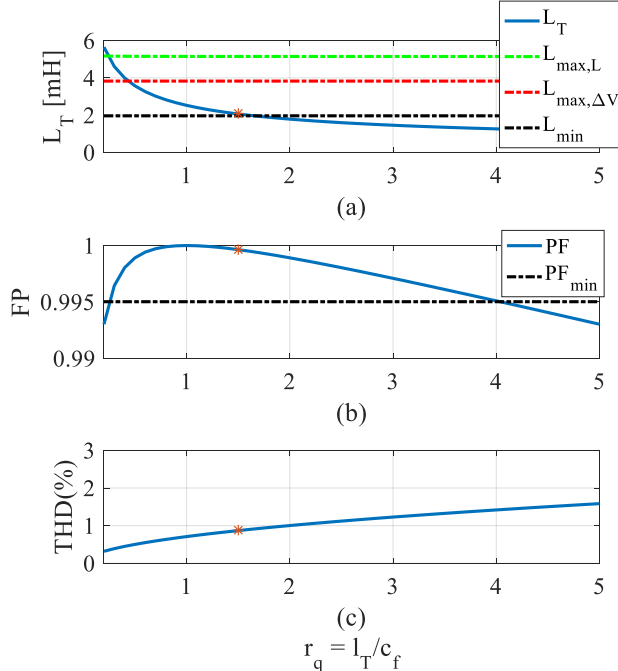


Fig. 2. Variation in the filter parameters for r_q : (a) Total filter inductance L_T ; (b) Power factor PF ; (c) Grid current THD .

Table IV. Parameters of the designed LCL filter.

Parameter	Symbol	Value
Converter side inductance	L_f	1 mH
Grid side inductance	L_g	1 mH
Filter Capacitance	C_f	14.8 μF
Filter power factor	PF	0.9996
Grid current THD	THD	0.87 %

2.4. Effect of losses of inductors in resonance peak

In fact, the losses of inductors insert some damping in the filter resonance frequency. However, the inductances are designed to have small losses and, unfortunately, a small damping is inserted into the system. This subsection aims to analyze this effect using the parameters designed in section 2.7 and presented in Table IV.

Considering that inductor losses can be modeled as a resistance in series with the inductance, the transfer functions $G_{if}(s) = I_f(s)/V_f(s)$ and $G_{ig}(s) = I_g(s)/V_f(s)$ presented in Table I will be transformed into:

$$G_{if}(s) = \frac{s^2 C_f L_g + s C_f R_g + 1}{s^3 C_f L_g L_f + s^2 C_f (L_f R_g + L_g R_f) + s (C_f R_g R_f + L_f + L_g) + R_f + R_g}, \quad (14)$$

$$G_{ig}(s) = \frac{1}{s^3 C_f L_g L_f + s^2 C_f (L_f R_g + L_g R_f) + s (C_f R_g R_f + L_f + L_g) + R_f + R_g}, \quad (15)$$

respectively. R_f and R_g are the resistances of the inductors L_f and L_g respectively.

The Bode diagrams of these transfer functions for some values of inductor X/R ratio are presented in Fig. 3 (a) and (b). This ratio was calculated at the fundamental frequency. The resistance of inductors has an impact mainly on the low-frequency region and a less expressive impact on the resonance frequency region. It is possible to observe that even for small X/R , the resonance peak is still evident and damping strategies are necessary. Additionally, most studies in literature design the damping strategies considering ideal inductors, since this is the worst case in terms of stability for the control system [54]. A $X/R = 40$ ratio is considered for all analyses presented in this study.

These bode diagrams also help to understand why the inverter current presents a larger ripple and harmonic distortion than grid current. In fact, the filter design considers the switching frequency larger than resonance frequency. Since transfer function $G_{ig}(s)$ presents a larger attenuation than $G_{if}(s)$, the harmonic distortion of grid current i_g is smaller than the inverter current i_f .

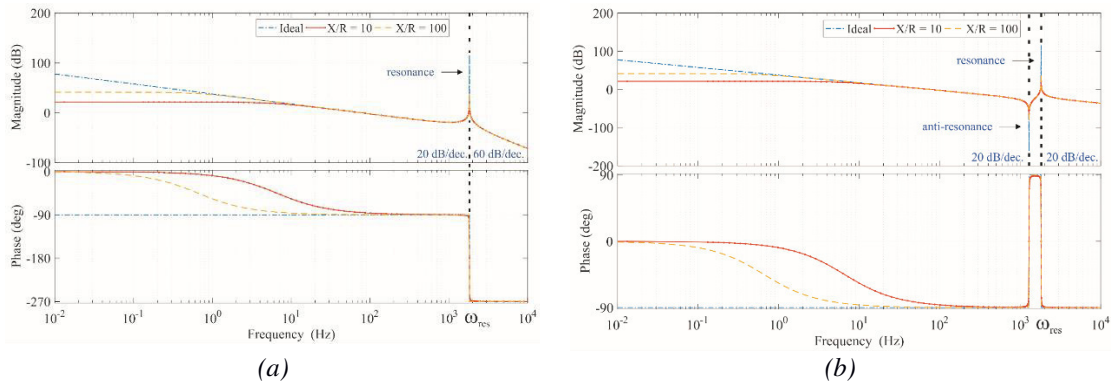


Fig. 3. Effect of the inductor X/R ratio in the LCL filter frequency response: (a) $G_{ig}(s)$ Bode diagram; (b) $G_{if}(s)$ Bode diagram.

3. Control strategies of Grid-connected inverters

Most applications of three-phase voltage-source converters present a control structure including an internal current loop. The also-called current control mode strategy is preferred because it softens the current dynamic behavior. Thereby, current control mode tends to protect the converter semiconductor switches [62].

Furthermore, for a grid-connected inverter, the dc bus voltage needs to be regulated and the injected current needs to be in synchronism with the grid voltage. Considering this approach, the converter control needs to measure the following variables: three-phase currents, three-phase voltages and dc bus voltage. The control of injected reactive power is also possible. Additionally, ancillary services, such as grid voltage support, power curtailment, unbalance and harmonic compensation can be included in the control algorithm [34].

When the converter is interfaced by a LCL filter, there are several possibilities to use voltage and current sensors. Reference [28] concludes that measuring the PCC voltages instead of the filter capacitor voltages improves grid synchronization. This improvement is justified by the harmonic components of the capacitor voltage, which will reflect in the control performance. For this reason, most studies in literature consider three high precision sensors to measure the grid voltage in order to synchronize the converter. Furthermore, the grid voltage can be used in the control strategy, as a feedforward term, thus improving the current control dynamic performance [28]. Some works in literature [36,63,64] propose the estimation of the line voltage in order to reduce the number of sensors. However, these strategies increase the complexity and the dependence of the control strategy from system parameters [16].

Whereas the injected grid currents are sinusoidal signals, conventional proportional-integral (PI) controllers in abc coordinates do not have a good performance. The limited gain of PI controllers results in steady-state errors in terms of amplitude and phase of current references [62]. Therefore, other control strategies are related in literature in order to solve this problem, including:

- Sliding-mode based controllers [65,66];
- Passivity-based controllers [67–69];
- Repetitive controllers [70–72];
- Fuzzy logic based controllers [73–75];
- Dead-beat controllers [76–78];
- Resonant controllers [40,41,79,80];
- Proportional integral controllers [14–17,24,32,54].

Nevertheless, the strategies most employed in the industry are PI controllers in synchronous reference frame (dq) or the use of proportional-resonant (PR) controllers in stationary reference frame ($\alpha\beta$) [34]. In terms of theoretical dynamic behavior, the techniques are similar, since PI controllers in synchronous reference frame are almost equivalent to PR controllers in stationary reference frame, as stated in [40].

When the control is implemented in synchronous reference frame, it is necessary an accurate estimate of grid voltage phase angle. This task is generally solved by means of a phase-locked loop (PLL) structure. A robust PLL needs to be able to reject grid disturbances, such as unbalanced voltage dips and harmonics. For three-phase systems, the double second order generalized integrator PLL (DSOGI-PLL) proposed by [81], and the decoupled double synchronous reference frame PLL (DDSRF-PLL) proposed by [82] are the most used in literature.

On the other hand, when the control strategy is implemented in stationary reference frame, the digital implementation of PR controller requires some caution. Proper discretization techniques should be used in order to guarantee the control performance, mainly when low sampling frequency is employed [79,80].

Additionally, two possibilities of current control can be explored: grid current feedback or converter current feedback. In both approaches, 2 or 3 high precision current sensors are used. According to [28], converter current measurements are justified in converter of kW-MW because the filter is not generally integrated in these converters. Thereafter, in order to maintain the current sensor integrated in the converter, current

measurement needs to be done on the converter side, which results in a more effective over-current protection [54].

On the other hand, reference [38] suggests the measurement of the grid currents, since the voltage sensors are already installed after the filter and, therefore, it can not be integrated in the inverter. Furthermore, this reference suggests the installation of high-precision sensor to measure the grid current and low-precision current sensors in the converter side, only for over-current protection.

Considering grid current control, according to [48], it is possible to yield stability without any damping strategy, if the filter parameters and the switching frequency are carefully designed. Nevertheless, the bandwidth of the system needs to be reduced, which results in poor dynamic behavior. For converter current control, reference [83] proposes a control strategy for a PV inverter without any damping strategy. A stable control system is also obtained by means of resonant controllers. However, the control bandwidth is limited and low order harmonics appear in the injected current.

Reference [29] presents a deep comparison between converter current and grid current feedback. It was observed that the performance of the current control is strongly related to the ratio between sampling and resonance frequencies, and also with the delay inserted by digital implementation. Furthermore, it is shown that the converter current feedback strategy requires an extra damping method while grid current feedback is stable. On the other hand, according to [31], the converter current is the superposition of the grid-side and capacitor filter currents. This relation explains how the feedback of the converter-side current provides an inherent damping, resulting in greater stability, if correctly explored.

Additionally, reference [84] shows mathematically the limits for current control stability. The discrete time domain model of the system is studied and three distinct regions of LCL filter resonance are defined: a high resonant frequency, a critical resonant frequency and a low resonant frequency region. The critical frequency corresponds to a relation between the switching and resonance frequency equal to $r_f = 6$. However, only the grid current control is approached in this work.

Reference [85] extends the analysis presented in [84] and shows that the converter current feedback and grid current feedback have opposite stability behavior. According to [85], the values of r_f contained at the range $2 \leq r_f \leq 6$ results in a stable grid current feedback, while for converter current feedback, the damping is essential to reach stability. On the other hand, if $r_f > 6$ or $r_f < 2$, the converter current feedback is stable, while for the grid current feedback, a damping strategy is necessary to reach stability. It is important to highlight that the region $r_f < 2$ is not recommended in practical designs, since it reduces filter attenuation in the switching frequency. Additionally, according to [85], for any given LCL-filter design and system sampling frequency, there is always one current feedback control that is inherently stable without damping. Nevertheless, according to [50], due to variations in the filter parameter and under weak grid conditions, the current control can become unstable. This fact justifies the use of damping strategies in both grid and converter current feedback [38].

The block diagram shown in Fig. 4 refers to the inverter current control, considering both approaches. $G_p(s)$ refers to the LCL filter; and the transfer function $G_d(s)$ refers to the delay introduced by the control strategy digital implementation. $G_c(s)$ refers to a PI current controller, given by:

$$G_c(s) = k_p \frac{(1 + \tau_i s)}{\tau_i s}. \quad (16)$$

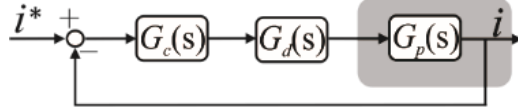


Fig. 4. Block diagram in z-domain for both grid and converter current control.

In general, the sampling and computation process can be modeled as a constant time delay δT_s , which is generally smaller than the sampling period T_s , i.e. $0 < \delta < 1$ [14,86]. Furthermore, there is another time delay of approximately $0.5T_s$ generated by the PWM computation and dead time, which can be modeled as a zero-order hold (ZOH) [87]. Therefore, the transfer function $G_d(s)$ can be represented as:

$$G_d(s) = e^{-s\delta T_s} \frac{1 - e^{-sT_s}}{s}, \quad (17)$$

where T_s is the sampling frequency.

Considering $\delta = 1$, the total delay inserted is approximately $1.5T_s$, which is frequently used in stability analysis [9,86]. In this situation, for the purposes of control design, $G_d(s)$ can be approximated by

$$G_d(s) \approx e^{-sT_d} \approx \frac{1}{sT_d + 1}, \quad (18)$$

where T_d is the total time delay, given by:

$$T_d = 1.5T_s. \quad (19)$$

The usual criterion for tuning the PI controllers is based on a first-order model of the LCL filter. This model is valid in the region of low frequencies, where the effect of the resonance is negligible [34]. This approach is very useful since it results in simple tuning formulas [14,15,34].

The complete model needs to be simplified so that low frequency models can be achieved. The LCL filter transfer function is given by (14), considering the converter current feedback, while for the grid current feedback, the LCL filter transfer function is given by (15). The Padé approximant is used in this work, as suggested in [15].

The Padé approximant of a function $f(x)$, denoted by $p_{M,N}(x)$ consists in a quotient of two polynomials with numerator degree N and denominator M , where $N > M$. Furthermore, $p_{M,N}(x)$ has the same Taylor series expansion of $f(x)$ up to degree $M + N$ [88]. The transfer functions considering Padé approximant in low-frequency region ($\omega \rightarrow 0$) for (14) and (15) are:

$$G_{if}|_{\omega \ll \omega_{res}} = \frac{1}{s(L_f + L_g - C_f R_g^2) + R_f + R_g}, \quad (20)$$

$$G_{ig} \Big|_{\omega \ll \omega_{res}} = \frac{1}{s(L_f + L_g + C_f R_g R_f) + R_f + R_g}. \quad (21)$$

Disregarding the high-order terms $C_f R_g^2$ and $C_f R_g R_f$, it is possible to write that:

$$G_{if} \Big|_{\omega \ll \omega_{res}} \approx G_{ig} \Big|_{\omega \ll \omega_{res}} \approx \frac{1}{sL_T + R_T}, \quad (22)$$

where $R_T = R_f + R_g$. This result can be also obtained by neglecting the capacitor branch at fundamental frequency, as suggested in [54].

Using the low frequency model given in (22), the tuning of the controllers is relatively simple. The open loop transfer function is given by:

$$G_{ol} = \frac{I(s)}{I_e(s)} = k_p \frac{(1 + \tau_i s)}{\tau_i s} e^{-sT_d} \frac{1/R_T}{1 + s \frac{L_T}{R_T}}. \quad (23)$$

The zero of the PI controller is used to cancel the dominant pole of the open loop transfer function. Therefore:

$$\tau_i = \frac{L_T}{R_T}. \quad (24)$$

In this situation, the open loop transfer function is given by:

$$G_{ol} = \frac{k_p}{\tau_i s} \frac{1}{R_T} e^{-sT_d} \approx \frac{k_p}{L_T s} \frac{1}{sT_d + 1}. \quad (25)$$

Therefore, the closed loop transfer function is given by:

$$G_{cl} = \frac{I(s)}{I^*(s)} = \frac{\frac{k_p}{L_T T_d}}{s^2 + \frac{1}{T_d} s + \frac{k_p}{L_T T_d}}. \quad (26)$$

The proportional gain is defined in terms of the desired damping in the closed loop dynamic. Considering the optimum technical method (closed loop damping factor equal to 0,707) [89], the proportional gain can be calculated by:

$$k_p = \frac{L_T}{3T_s}. \quad (27)$$

The phase margin (PM) and the gain margin (GM) of this adjustment can be determined by means of the absolute value and the angle of the open loop transfer function, given by:

$$|G_{ol}|_{s=j\omega} = \left| \frac{k_p}{sL_T} e^{-sT_d} \right| = \frac{k_p}{\omega L}, \quad (28)$$

$$\angle G_{ig}|_{s=j\omega} = -90^\circ - T_d \omega \frac{360^\circ}{2\pi}. \quad (29)$$

Therefore, the gain crossing frequency and phase crossing frequency are given by:

$$\omega_{gc} = \frac{k_p}{L_T}, \quad (30)$$

$$\omega_{pc} = \frac{\pi}{3T_s}, \quad (31)$$

which results in the following stability margins:

$$PM = 180^\circ + \angle G_{ol}|_{s=j\omega_{gc}} = 90^\circ - \frac{T_s k_p}{L} \frac{270^\circ}{\pi} \approx 61.4^\circ. \quad (32)$$

$$GM = |G_{ol}|_{s=j\omega_{pc}} = \frac{k_p}{\omega_{pc} L} = \pi \approx 9.94 dB. \quad (33)$$

Finally, the control bandwidth obtained through this adjustment is given by [14,15]:

$$f_{bw} \approx \frac{k_p}{2\pi L_T} \approx \frac{f_s}{20}. \quad (34)$$

4. Resonance damping strategies

The modeling and design of the following resonance damping strategies are developed in this section:

- Passive damping based on series resistor;
- Capacitor current feedback based method;
- Capacitor voltage feedback based method;
- Notch filter based method.

Fig. 5 presents the control strategies for each resonance damping method, which are described as follows.

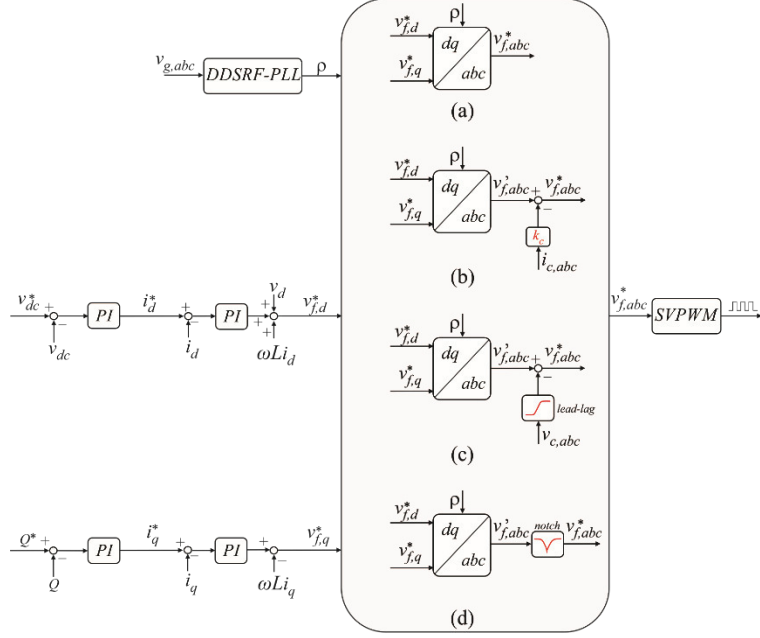


Fig. 5. Control Strategies in synchronous reference frame for some damping strategies: (a) Passive damping strategy; (b) Capacitor current feedback based strategy; (c) Capacitor voltage feedback based strategy; (d) Notch filter based strategy.

4.1 Passive damping (PD)

Passive damping is the most used method to reach stability in VSC based on LCL filters [17]. This technique consists in the insertion of some passive elements into the filter structure in order to change the filter response around the resonance frequency. Therefore, any additional sensors or modifications in the control structure are necessary, if compared with VSC based on L filters. This technique provides a simple and cost effective solution [30]. Nevertheless, passive damping generates additional losses in the filter and can compromise filter attenuation [14,17,22].

According to [5], the passive damping strategies can be sorted into three groups:

- Series passive damping (SPD) [14,17,22,28,30,54,56];
- Parallel passive damping (PPD) [34,90];
- Complex passive damping schemes (CPD) [5,17,22,58,91–93].

The series passive damping is an approach commonly found in literature and consists in the insertion of a resistor in series with the capacitor branch. This approach is presented in Fig. 6 (a). Small values of R_d are necessary to reduce losses. The transfer functions of the LCL filter, disregarding the inductors resistance, are given by:

$$G_{if,SPD} = \frac{1}{L_f s} \frac{s^2 + 2\zeta' Z_{LC} s + Z_{LC}^2}{s^2 + 2\zeta \omega_{res} s + \omega_{res}^2}, \quad (35)$$

$$G_{ig,SPD} = \frac{1}{L_f s} \frac{Z_{LC}^2 (C_f R_d s + 1)}{s^2 + 2\zeta \omega_{res} s + \omega_{res}^2}, \quad (36)$$

where $\zeta' = R_d C_f Z_{LC} / 2$ and

$$\zeta = \frac{C_f \omega_{res}}{2} R_d. \quad (37)$$

As observed in (36), the grid current attenuation is reduced for passive damping, since an additional zero is included in this transfer function due to series passive damping.

Generally $\zeta \ll 1$, it is necessary to limit the losses. In terms of design, reference [17] suggests that the maximum value of damping resistor is limited to the impedance of the capacitor at the switching frequency. Therefore,

$$R_{d,max} = \frac{1}{2\pi f_s C_f}. \quad (38)$$

On the other hand, $R_{d,min}$ is determined in order to guarantee stability in closed loop. According to [17], this minimum value can be approximated by:

$$R_{d,min} = \frac{1}{6\pi} \frac{L_g}{L_f} \frac{f_s}{f_{res}} \frac{1}{C_f \omega_{res}}. \quad (39)$$

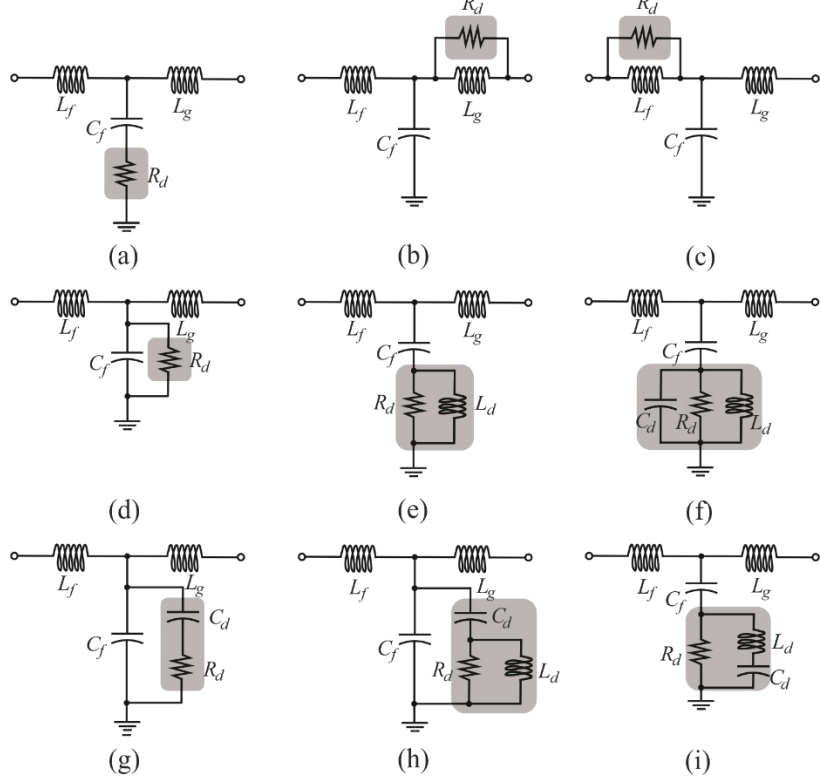


Fig. 6. Passive damping strategies: (a) Series passive damping; (b)-(d) Parallel passive damping; (e)-(i) Complex passive damping structures.

Considering $f_s \approx 3f_{res}$ and $L_g/L_f < 2$, the minimum value is approximately 20 % of the capacitor impedance at resonance frequency. This result is coherent with reference

[54], which suggests a resistance value equal to one third of the capacitor impedance at the resonant frequency in order to obtain good compromise between filter attenuation, stability and power losses.

A parallel passive damping consists of inserting a parallel resistor into the filter structure in order to improve the system stability. Three possibilities of parallel passive damping are presented in Fig. 6 (b)–(d). According to the reference [90], the approach presented in Fig. 6 (b) results in the best dynamic performance, disturbance rejection capability and high frequencies attenuation. Furthermore, high values of R_d needs to be employed to reduce losses [34].

Based on the approach of Fig. 6 (b), the LCL filter transfers functions, considering that both converter and grid current control are given by:

$$G_{if,PPD} = \frac{1}{L_f s} \frac{s^2 + 2\xi' Z_{LC}s + Z_{LC}^2}{s^2 + 2\xi\omega_{res}s + \omega_{res}^2}. \quad (40)$$

$$G_{ig,PPD} = \frac{1}{L_f s} \frac{Z_{LC}^2 \left(\frac{L_g}{R_d} s + 1 \right)}{s^2 + 2\xi\omega_{res}s + \omega_{res}^2}. \quad (41)$$

where $\xi' = (2C_f R_d Z_{LC})^{-1}$ and

$$\xi = \frac{1}{2\omega_{res} C_f R_d}. \quad (42)$$

The parallel passive damping method also reduces filter attenuation, since this method adds a zero in the LCL filter transfer function. The design of this method is based on root-locus analysis in discrete time domain. More details can be found in [90].

Power losses are an important issue in medium and high power applications [3,22]. In this situation, some works propose the use of complex passive damping strategies, in order to reduce the power losses introduced by the series passive elements. In fact, the losses in the damping resistor can be sorted into two sources: fundamental and high order harmonics. Reference [91] proposes to install an inductance in parallel with the damping resistor, as illustrated in Fig. 6 (e). This inductance is designed to provide a low impedance path ($\omega_n L_d \ll R_d$) thus reducing considerably the losses due to the fundamental component. Under such conditions, low frequency components will flow through the low impedance branch generated by the inductance.

According to [17], the value of the inductance L_d is designed considering that the impedance ratio at fundamental and resonance frequencies are equal. Thereby,

$$L_d = \frac{R_d}{\sqrt{\omega_f \omega_{res}}}. \quad (43)$$

Thereafter, the topology presented in Fig. 6 (f) was proposed by [22] in order to reduce the losses generated by the switching harmonics. The capacitance C_d is designed to provide a low impedance path for the switching frequency harmonics. Nevertheless, at the resonance frequency, the resistor impedance needs to be dominant, for proper damping. Under these conditions, according to [17], the value of the capacitance can be obtained by:

$$C_d = \frac{1}{R_d \sqrt{\omega_{res} \omega_s}}. \quad (44)$$

Additionally, reference [58] proposes a shunt $C_d - R_d$ branch, as shown in Fig. 6 (g). The design of the ratio between the capacitances $r_c = C_f/C_d$ directly affects the filter frequency response. Reference [58] suggests $r_c = 1$, which results in a tradeoff between the damping and power losses.

An improved passive damping scheme was proposed by [92], as presented in Fig. 6 (h). This approach includes an inductance L_d in parallel with the damping resistor, reducing the losses for the fundamental current. Finally, reference [93] proposes the scheme presented in Fig. 6 (i). This scheme includes a branch composed by an inductance and capacitance. This LC branch is tuned in the switching frequency, which results in a low impedance path for high frequency components and minimizes the losses [5].

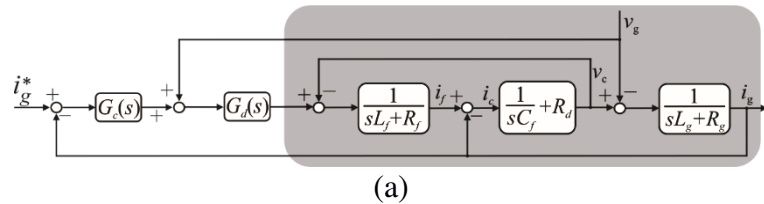
Alternatively, additional computational delay in the control algorithm has a positive impact on stability. Using this strategy, the necessary value of damping resistor to obtain stability is approximately 50 % of the value used in the conventional approach, which reduces power losses [4,17]. However, the bandwidth is reduced (approximately 60 %) when this delay is included, as stated in [4].

Transfer functions for some complex passive damping strategies can be found in [30]. It is important to observe that complex passive damping methods increase the order of the control system and affect the complexity of the controller design. The comparison of these methods in terms of losses and total harmonic distortion is presented in [14]. Furthermore, a study comparing losses in the desired damping factor is presented in [34]. For the sake of simplicity, the present review focuses on series passive damping. However, the analysis presented here can be extended for all passive damping strategies in further works.

The block diagrams of series passive damping control strategies, considering both converter and grid current control, are presented in Fig. 7. In terms of control design, the same gains designed in section 3 are used, since the series passive damping does not affect the Padé approximants of (20) and (21).

The root locus in the z -plane of the closed loop poles, which is used in this work, is very useful [14], for the design of the passive damping resistor and it is used by this work. Fig. 8. presents the block diagram in z -domain, considering a current control strategy with passive damping Fig. 8. $G_p(z)$ is resultant from the plant transfer function discretization (dependent on current control), based on the zero-order hold method. Under these conditions, the closed loop transfer function is given by:

$$H(z) = \frac{G_c(z)G_p(z)}{z + G_c(z)G_p(z)}. \quad (45)$$



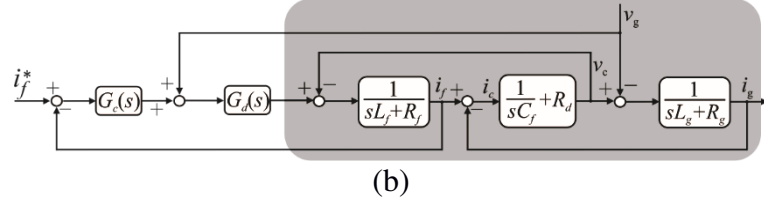


Fig. 7. Block diagram for current control strategy based on series passive damping: (a) Grid current control; (b) Converter current control.

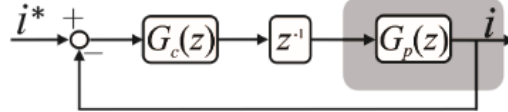


Fig. 8. Block diagram in z -domain for both grid and converter current control.

Using the parameters of Table IV, the root locus in the z -plane as function of the resistance R_d is plotted in Fig. 9 for three control strategies discussed before: Grid current control, converter current control and converter current control with additional delay. As observed in Fig. 9 (a), the grid current control presents stable behavior even without damping. When the passive damping resistor is increased, the damping and losses obtained also increase. Reference [4] suggests $\zeta = 0.1$, which results in $R_d = 0.3\Omega$ (red point).

On the other hand, the converter current control is unstable without damping, as shown in Fig. 9 (b). In order to obtain the same damping of the grid current control, it is necessary a damping resistor equal to $R_d = 2.7\Omega$. Therefore, grid current control tends to reduce the losses caused by passive damping.

Finally, the insertion of an additional computational delay in current control has a positive impact on stability, since resistance to reach the same damping is $R_d = 1.7\Omega$, almost half of the previous strategy, as shown in Fig. 9 (c). Nevertheless, an additional pole is included in the root locus analysis and the passive damping is slightly affected. Then, the additional delay tends to reduce the control bandwidth, as mentioned before.

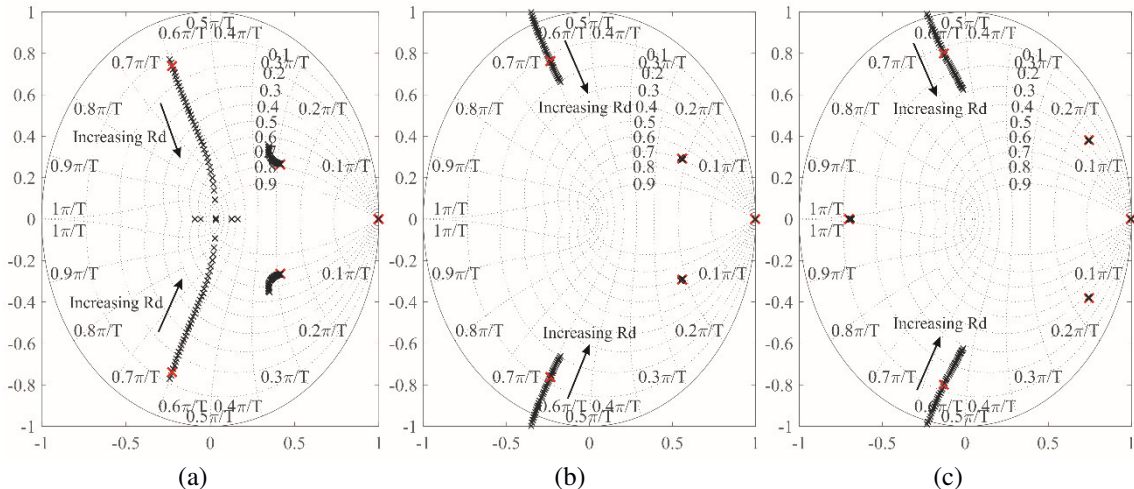


Fig. 9. Root locus in z -plane by varying damping resistor R_d for: (a) Grid current feedback; (b) Converter current feedback; (c) Converter current feedback with additional computational delay.

4.2 Capacitor current feedback (CCF)

The capacitor current feedback strategy was proposed by [40]. This method is also called virtual resistor method, since it results in damping similar to that of the series passive damping [5]. This strategy includes a feedback of the capacitor current into the current control, providing an additional damping in the closed loop. The block diagram of this strategy is presented in Fig. 10 (a) and (b) for both converter and grid current control, respectively.

As observed in Fig. 10, the CCF block diagram can be interpreted as a cascade current control [94]. Even the inner loop is composed of a simple proportional gain. In order to stabilize the control system, its steady-state error does not affect the outer loop accuracy [40]. Other topologies of controllers (integral and derivative controllers) were approached in [32]. However, the proportional controller presented the best results for stability and dynamic behavior.

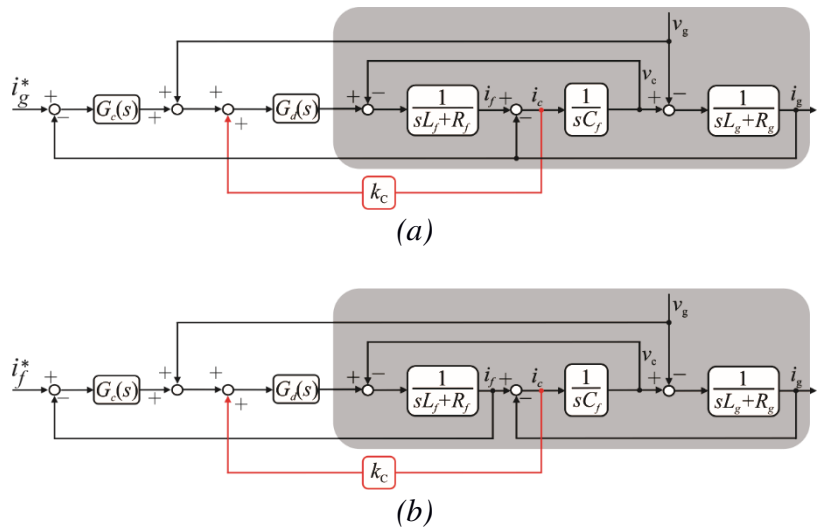


Fig. 10. Block diagram for current control strategy based on capacitor current feedback: (a) Grid current control; (b) Converter current control.

The LCL filter transfer function, considering the capacitor current feedback is given by [14,15]:

$$G_{if,CCF} = \frac{1}{L_f} \frac{s^2 + Z_{LC}^2}{s^2 + 2\zeta_c \omega_{res}s + \omega_{res}^2}, \quad (46)$$

$$G_{ig,CCF} = \frac{1}{L_f} \frac{Z_{LC}^2}{s^2 + 2\zeta_c \omega_{res}s + \omega_{res}^2}, \quad (47)$$

where $\zeta_c = \frac{k_c}{2L_f \omega_{res}}$. As observed in (47), active damping technique does not insert zeros in the filter transfer function. Therefore, it does not affect filter attenuation. Thereby, the

obtained damping in closed loop is related with the feedback gain k_c . This gain is smaller than twice the converter inductance impedance at the resonance frequency, in order to guarantee $0 \leq \zeta \leq 1$.

As mentioned before, the ratio between the switching and resonance frequency r_f affects directly the performance of the active damping strategies. The analysis of the capacitor current feedback technique as function of r_f was presented by [32]. It was concluded that the capacitor current has a good performance for high and medium values of r_f . Additionally, references [14,95] show mathematically, by different forms, that the ratio $r_f \approx 3$ minimizes the effect of the computational delay in the control system.

Generally, the gain k_c is adjusted in terms of the desired damping in closed loop. This gain needs to be adjusted with great caution, since small values cannot damp the resonance effectively and large values may result in system instability [29,41]. Reference [41] proposes a design methodology in order to determine the parameters of the PI controller and the active damping gain so as to maximize the stability margins and crossover frequency. Alternatively, the compensators can be designed based on Padé approximant. The Padé approximants for LCL filter, considering CCF damping strategy for converter and grid current control, are given by:

$$G_{if}|_{\omega \ll \omega_{res}} = \frac{1}{s(L_f + L_g - C_f R_g^2 + k_c C_f R_g) + R_f + R_g}, \quad (48)$$

$$G_{ig}|_{\omega \ll \omega_{res}} = \frac{1}{s(L_f + L_g + C_f R_f R_g + k_c C_f R_g) + R_f + R_g}, \quad (49)$$

which are very similar to the Padé approximant presented in (20) and (21), since additional terms are very small [14].

Using the parameters of Table IV, the root locus in the z -plane in function of the CCF damping gain k_c is plotted in Fig. 11 (a)(b), for both grid and converter current control, respectively. As can be observed, the CCF based method affects both high and low frequency poles of the controlled system. Furthermore, in order to obtain the same damping, the gain considering the grid current control strategy is smaller than that of converter current control strategy.

Damping the resonance poles too much would not be appropriate, as it would result in excessive control effort [14]. Therefore, a damping factor equal to $\zeta = 0.1$ is used again [4], which results in $k_c = 0.1$ for grid current control and $k_c = 4$ for converter current control.

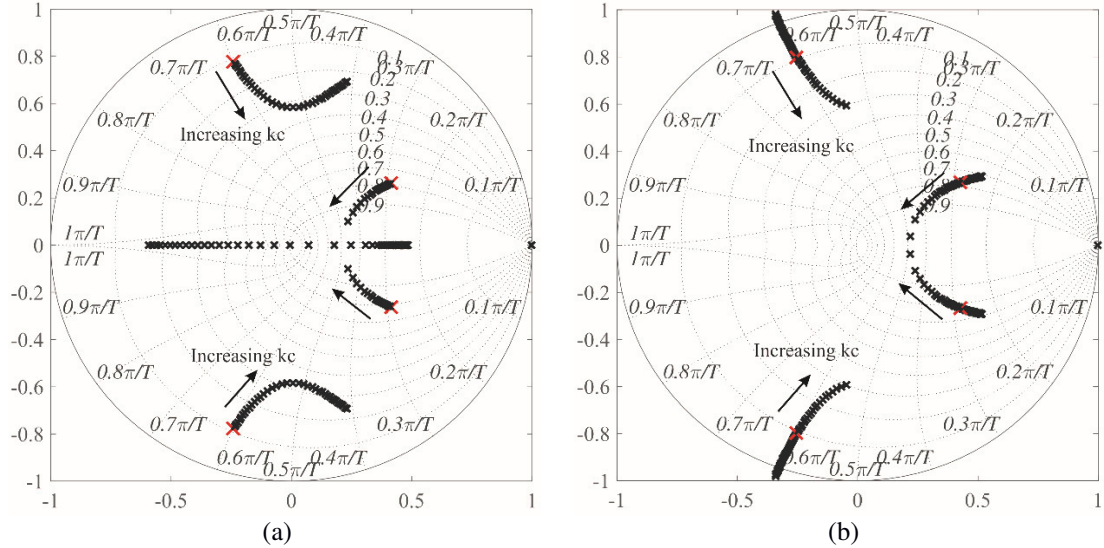


Fig. 11. Root locus in z-plane by varying the active damping gain k_c for: (a) Grid current feedback; (b) Converter current feedback.

4.3 Capacitor voltage feedback (CVF)

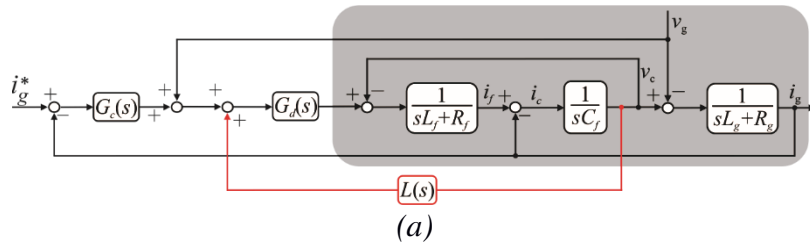
The capacitor voltage feedback strategy was proposed by [4]. This strategy includes a feedback of the capacitor voltage measurement in the current control, which results in additional damping in the closed loop. The block diagram of this strategy is presented in Fig. 12 (a) (b) for both converter and grid current control strategies, respectively.

The capacitor voltage or capacitor current feedback chosen is affected by economic factors. According to [32], for higher power levels (MW range, but at low voltages <1000 V), current sensors are much more expensive than voltage sensors. On the other hand, at low power (few kW range), standard current sensors might even be cheaper than voltage sensors with the same level of insulation. Furthermore, a reduced number of sensors can be used if the capacitor voltage is measured for both converter synchronization and active damping, if compared with CCF strategy [96].

Regarding the dynamic behavior, the CVF and CCF damping strategies are equivalent only if the transfer function $L(s)$ is given by:

$$L(s) = k_c C_f s. \quad (50)$$

Nevertheless, the implementation of an ideal differentiator transfer function is complex and can introduce noise in the control system. Reference [96] presents the limitations and discusses some alternatives to implement an approximate differentiator transfer function, including as: second order generalized integrator, non-ideal generalized integrator and lead-lag element. This latter is presented in many works in literature [4,14,15] and will be discussed in this section.



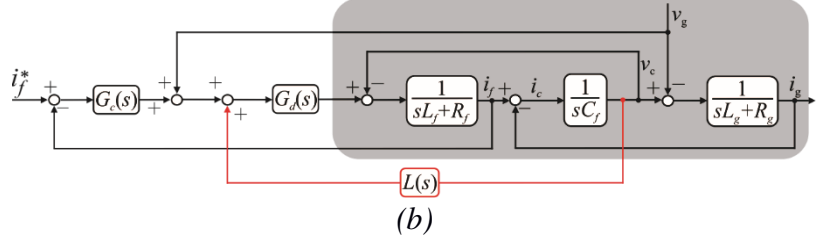


Fig. 12. Block diagram for current control strategy based on capacitor voltage feedback: (a) Grid current control; (b) Converter current control.

The lead-lag network transfer function for CVF strategy is given by:

$$L(s) = k_v C_f \omega_{max} \left(\frac{s + k_f \omega_{max}}{k_f s + \omega_{max}} \right), \quad (51)$$

where k_v is the gain tuned for active damping, ω_{max} is the frequency which results in maximum phase, k_f is a constant which defines the distance between zero and the pole of the lead-lag network. This constant can be calculated according to the maximum phase φ_{max} as:

$$k_f = \sqrt{\frac{1 - \sin\varphi_{max}}{1 + \sin\varphi_{max}}}, \quad (52)$$

The lead-lag element frequency response is compared with a perfect differentiator in Fig. 13. As observed, these transfer functions are similar in magnitude around the frequency ω_{max} . However, differences are observed for the phase, which will affect the dynamic behavior of the CVF damping strategy.

In order to approximate correctly the ideal differentiator around the resonance frequency and obtain φ_{max} as close as possible to 90° , it is considered that:

$$\omega_{max} = \omega_{res}. \quad (53)$$

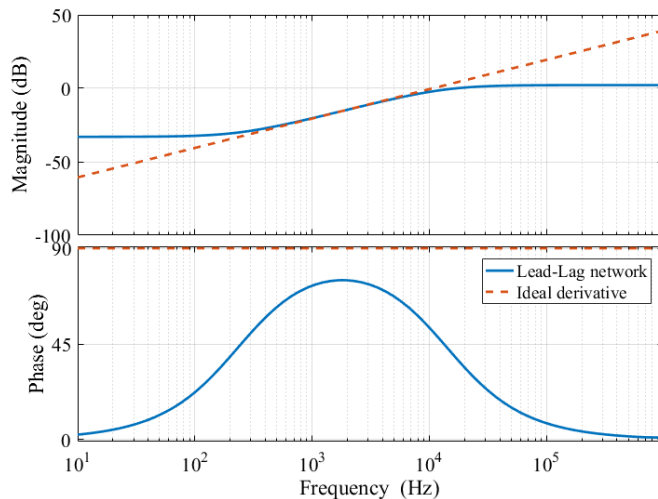


Fig. 13. Bode diagram comparison of lead-lag network and the ideal differentiator.

Regarding digital implementation, the lead-lag network needs to be discretized by using the Tustin method with pre-warping at ω_{res} [15,80]. This method will preserve the phase and the amplitude of this transfer function around the resonance frequency [79,80]. Furthermore, according to [15], the maximum phase is contained at the range $70^\circ \leq \varphi_{max} \leq 80^\circ$. Additionally, reference [14] shows mathematically that the ratio between the switching and the resonance frequency is at the range $3.2 \leq r_f \leq 3.4$, thus minimizing the effect of the computational delay on the control system.

The adjustment of the gain k_v is determined by the desired damping in closed loop. Small values of k_v cannot damp the resonance effectively and large values may result in system instability [4,15]. Generally, the root locus in the z -plane is used during the design process. According to [15], the lower value of k_v in order to keep the system stable, can be estimated by:

$$k_{v,min} = \frac{1}{3} \frac{L_g}{T_s}, \quad (54)$$

where T_s is the sampling period.

The compensators can be designed in terms of Padé approximant. The Padé approximant of the LCL filter, considering the CVF damping strategy, for converter and grid current control strategies, is given by:

$$G_{if}|_{\omega \ll \omega_{res}} = \frac{1}{s(L_f + L_g K_{ll} - C_f R_g^2 K_{ll}) + R_f + R_g K_{ll}}, \quad (55)$$

$$G_{ig}|_{\omega \ll \omega_{res}} = \frac{1}{s(L_f + L_g K_{ll} + C_f R_f R_g) + R_f + R_g K_{ll}}. \quad (56)$$

where

$$K_{ll} = 1 + H_{ll}(s)|_{s=0} = 1 + k_v k_f C_f \omega_{res}. \quad (57)$$

Neglecting the high order terms, the Padé approximant of the LCL filter, considering the CVF damping strategy, can be written as follows:

$$G_i|_{\omega \ll \omega_{res}} \approx \frac{1}{s L_{eq} + R_{eq}}, \quad (58)$$

where $L_{eq} \approx L_f + L_g K_{ll}$ and $R_{eq} \approx R_f + R_g K_{ll}$. The PI compensators are designed using the equivalent inductances L_{eq} and R_{eq} instead of L_T and R_T .

However, according to [4], this control adjustment can result in an overshoot higher than the expected 4 % to the step response. In this situation, reference [15] suggests the reduction of the PI controller proportional gain. In fact, if the proportional gain is reduced by half, the closed-loop dominant poles become critically damped and the resultant overshoot will be a function of the high frequency dynamics. Therefore, if the overshoot is not acceptable, k_p should be reduced, but not as much as halving (27). Unfortunately, this reduction directly affects the control bandwidth, as suggested by (34).

Using the parameters of Table IV and considering $\varphi_{max} = 75^\circ$, the root locus in the z -plane in function of the CVF damping gain k_v is plotted in Fig. 14, for both grid and converter current control. It can be observed that the CVF based method affects both the high and low frequency poles of the controlled system.

Furthermore, in order to obtain the same damping, the gain of grid current control strategy is smaller than in the case of converter current control strategy. Additionally, the gain k_v cannot be increased much, since large values of k_v lead to closed loop instability. Considering again a damping factor equal to $\zeta = 0.1$ [4], the active damping gain is $k_v = 0.1$ for grid current control strategy and $k_v = 4.5$ for converter current control strategy.

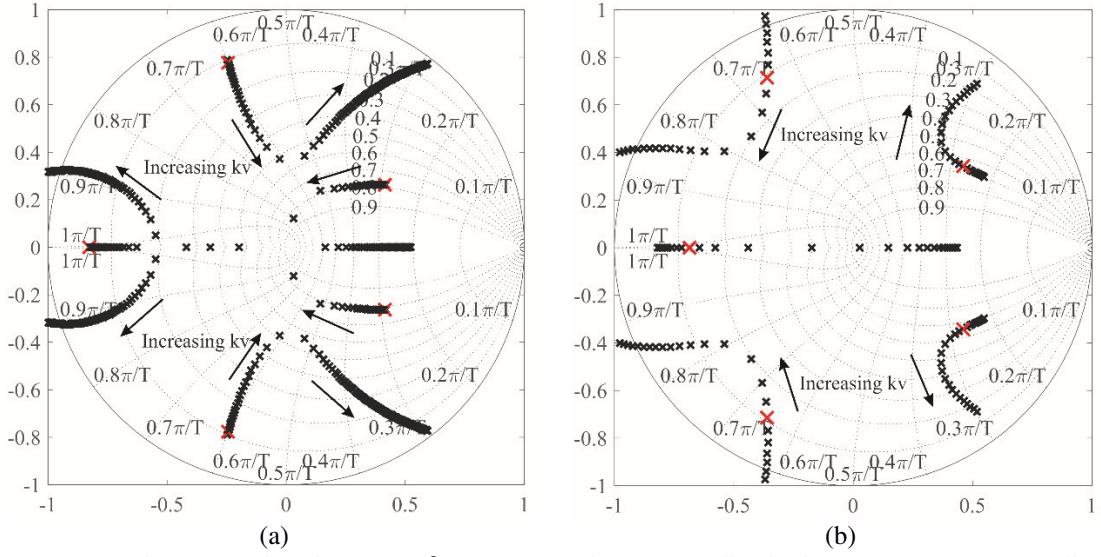


Fig. 14. Root locus in z -plane by varying k_v for: (a) Grid current feedback; (b) Converter current feedback.

4.4 Notch Filter (NF)

In the notch-filter based active damping strategy, a notch transfer function $N(s)$ is inserted in series with the current controller, as presented in Fig. 15 (a) (b) for grid and converter current feedback strategies, respectively. This technique is relatively simple to implement since it does not require additional sensors. Reference [24] compares 3 strategies of filter-based active damping methods: low-pass filter, lead-lag element and notch filter. It was concluded that the notch-filter solution is the most flexible and effective strategy.

This strategy aims to compensate the LCL filter resonance by means of the notch filter anti-resonance. The generic transfer function of a notch filter is given by [16,86]:

$$N(s) = \left(\frac{s^2 + 2\xi_{nz}\omega_{nf} + \omega_{nf}^2}{s^2 + 2\xi_{np}\omega_{nf} + \omega_{nf}^2} \right)^n, \quad (59)$$

where ω_{nf} is the anti-resonance frequency and n refers to the number of sections inserted. ξ_{nz} and ξ_{np} are the damping factors of the filter zeros and poles, respectively.

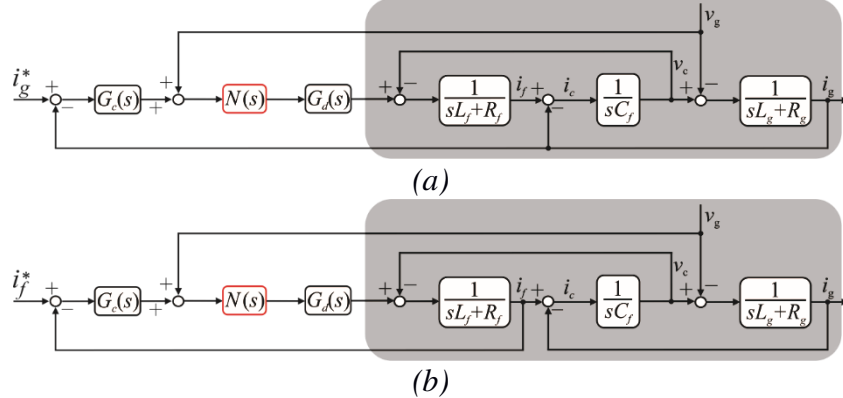


Fig. 15. Block diagram for current control strategy based on notch filter: (a) Grid current control; (b) Converter current control.

In order to obtain a stable system, with a positive gain margin, it is necessary to analyze if the open loop transfer function has gain below 0 dB at the resonance frequency. Therefore:

$$G_c(s)G_d(s)G_p(s)N(s)|_{s=j\omega_{res}} < 1 \Rightarrow \frac{\xi_{nz}}{\xi_{np}} < \frac{1}{|G_c(s)G_d(s)G_p(s)|}. \quad (60)$$

Generally, the settings $\xi_{nz} = 0$ and $\omega_{nf} = \omega_{res}$ are preferred in order to achieve absolute cancellation at resonance frequency, even when digital implementation of notch filter is considered. In this case, the relation (60) is always fulfilled [16]. Additionally, the discretization of the notch transfer function needs to be based on the Tustin method with prewarping, in order to maintain the magnitude and phase characteristics around the resonance frequency [79,80]. Additionally, reference [86] explores the inherent damping characteristics of the LCL filter and proposes to allocate the notch filter frequency ω_{nf} , in a different position of the resonance frequency ω_{res} , in order to increase the robustness of the damping strategy for grid inductance variation.

The effect of the damping factor ξ_{np} in notch-filter transfer function is presented in Fig. 16 (a). As observed, small damping factors result in a narrow notch of the filter and reduce the phase lag introduced in the low frequency region. Additionally, the number of sections n has a larger effect in the filter notch band, as observed in Fig. 16 (b). It is important to point out that narrow bandwidth increases sensibility to the variations in the resonance frequency [86,97].

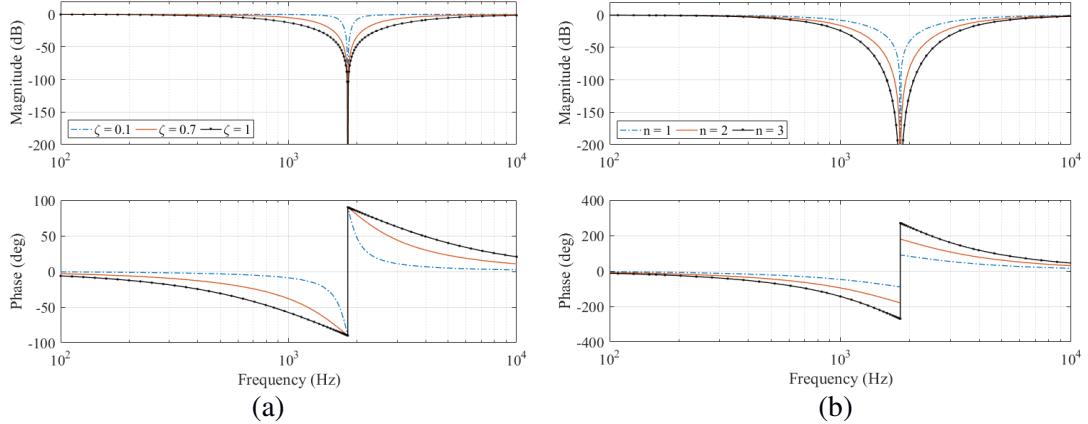


Fig. 16. Bode diagrams for notch filter as function of main parameters: (a) Effect of damping factor ξ_{np} ; (b) Effect of the number of sections n .

The notch filter phase-lag can cause instability in the current control strategy, since it introduces an important phase lag in the current control. Once current control loop behaves almost like a second order system, the phase margin and the closed loop damping are approximately proportional. Therefore, a decreased phase margin reduces the damping factor and increases the overshoot in the current control loop. Thereby, this issue needs to be approached. The Padé approximant of a notch filter for $\omega \ll \omega_{nf}$ is given by:

$$N(s)|_{\omega \ll \omega_{nf}} = \left(\frac{1}{\tau s + 1} \right)^n, \quad (61)$$

where $\tau = \frac{2(\xi_{np} - \xi_{nz})}{\omega_{nf}}$. Using the Padé approximant and applying Taylor series, the amplitude and the phase of the notch filter in low frequency can be estimated by [16]:

$$|N(j\omega)| \approx -\frac{40}{ln 10} n (\xi_{np} - \xi_{nz})^2 \left(\frac{\omega}{\omega_{nf}} \right)^2, \quad (62)$$

$$\angle N(j\omega) \approx -2n (\xi_{np} - \xi_{nz}) \left(\frac{\omega}{\omega_{nf}} \right), \quad (63)$$

As observed, whereas the relation $\frac{\omega}{\omega_{nf}}$ is reduced, the effect on the phase becomes more significant on the magnitude. Therefore, the gain crossover frequency is slightly affected, while the phase margin changes significantly. In fact, the phase margin is reduced in comparison with the low frequency model, due to the notch filter delay. Considering $\xi_{nz} = 0$, the damping factor can be adjusted as function of the phase margin reduction Δ_{PM} as:

$$\xi_{np} = \frac{1}{2} \tan \left(\frac{\Delta_{PM}}{n} \right) \frac{\omega_{nf}}{\omega}. \quad (64)$$

As observed, for small Δ_{PM} , $\tan \theta \approx \theta$, and the number of sections n tends to decrease Δ_{PM} for the same damping. However, the increase of n tends to increase the complexity of the filter digital implementation [16].

Decreased phase margin can be compensated by reduced controller proportional gain. Nevertheless, this reduced gain results in a lower bandwidth, as suggested by (34). A lower bound for the reduced gain can be estimated by (32) and is given by:

$$k_p(\%) = 100 \left(1 - \frac{\pi}{90} \Delta_{PM} \right) \quad (65)$$

where $k_p(\%)$ is the percentage value of the new proportional gain. For example, in order to limit the bandwidth reduction in 50%, the phase margin variation cannot be greater than 15° [16].

The phase lag inserted by notch filter is critical for converter current control and has a large effect on the stability. Therefore, reference [16] suggests the use of $n = 2$. The phase lag is not critical for grid current control, since the control is inherently stable. Thereby, reference [97] suggests the use of $n = 1$ in order to reduce the control computational effort.

Additionally, the Padé approximants of the control plant, considering the notch filter, are given by:

$$G_{if}|_{\omega \ll \omega_{res}} = \frac{1}{s[L_f + L_g - C_f R_g^2 + +\tau(R_f + R_g)] + R_f + R_g}, \quad (66)$$

$$G_{ig}|_{\omega \ll \omega_{res}} = \frac{1}{s[L_f + L_g + C_f R_f R_g + \tau(R_f + R_g)] + R_f + R_g}. \quad (67)$$

which are very closed to the Padé approximant presented in (20) and (21), since additional terms are very small.

Using the parameters of Table IV, the root locus in the z -plane in function of the notch filter damping gain ξ_{np} is plotted in Fig. 17. As can be observed, the NF based method affects both the high and low frequency poles of the controlled system. The increased impacts of ξ_{np} on the damping of dominant poles increased the overshoot, as aforementioned.

Furthermore, in order to obtain the same damping, grid current control strategy has smaller ξ_{np} than the converter current control strategy. For grid current control strategy, $\xi_{np} = 0.1$ is sufficient, while for the converter current control strategy, $\xi_{np} = 0.5$ is necessary.

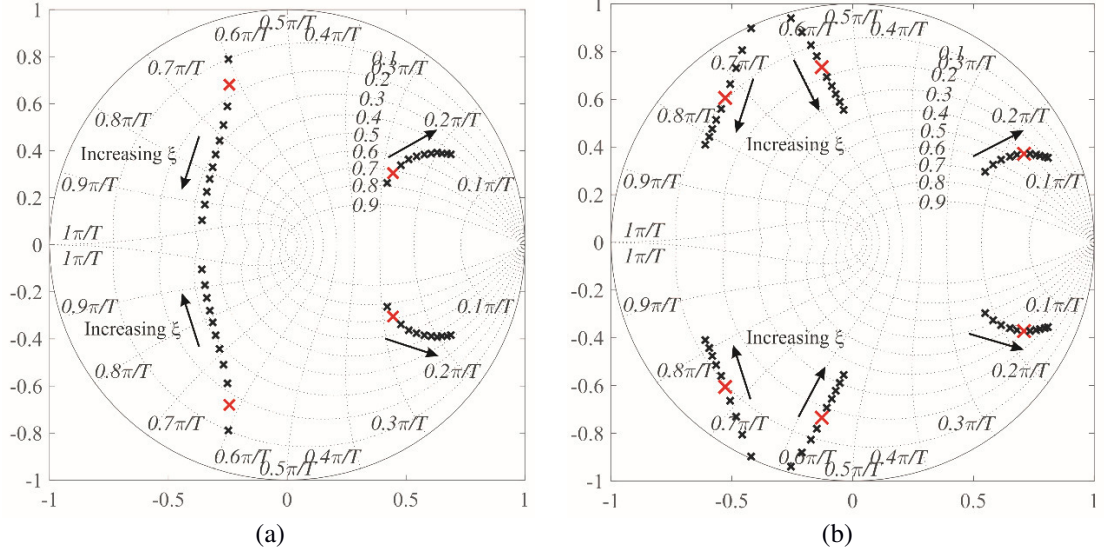


Fig. 17. Root locus in z -plane by varying the damping factor ξ_{np} for: (a) Grid current feedback; (b) Converter current feedback.

Finally, an overview of the design constraints of the four strategies aforementioned are described in Table V. Next section presents the results obtained for the case study proposed in this work.

Table V. Overview of the design guidelines for the damping strategies approached in this work.

Damping Strategy	Pade Aprox.	$r_f = \frac{f_s}{f_{res}}$	Design constraints
PD	Eq. (20) - i_f Eq. (21) - i_g	$r_f \approx 4.5$	$\frac{1}{6\pi} \frac{L_g}{L_f} \frac{f_s}{f_{res}} \frac{1}{C_f \omega_{res}} \leq R_d \leq \frac{1}{2\pi f_s C_f}$
CCF	Eq. (48) - i_f Eq. (49) - i_g	$r_f \approx 3$	$k_c \leq 2L_f \omega_{res} *$
CVF	Eq. (55) - i_f Eq. (56) - i_g	$r_f \approx 3.2 - 3.4$	$k_v \geq \frac{1}{3} \frac{L_g}{T_s} **$
NF	Eq. (66) - i_f Eq. (67) - i_g	$r_f \approx 4.5$	$n = 2, \omega_{nf} = \omega_{res}$ for i_f control $n = 1, \omega_{nf} = \omega_{res}$ for i_g control

* If $2 \leq r_f \leq 6$, grid current feedback is inherently stable; If $r_f > 6$, converter current feedback is inherently stable.
** The minimum value of k_c is related with the desired damping;
*** k_v needs to be defined carefully, since large values of k_v can make the system unstable.

5. Dynamic performance of the studied damping strategies

5.1 Time domain performance

In order to verify the behavior of the damping strategies designed previously, time domain simulations were developed in PLECS environment. In the presented results, a grid inductance equals to $1mH$ is considered. Additionally, the following events were implemented:

- Firstly, the PLL algorithm is executed in order to synchronize the converter to the grid;

- Then, the inverter is connected to the grid and the control system maintains the grid current at zero. For grid current control strategies, both direct and quadrature reference currents are maintained at zero. Therefore, $i_{d,g} = 0$ and $i_{q,g} = 0$. For converter current control, the direct reference current is maintained at zero, while the quadrature component is calculated to supply the filter reactive power. Therefore, $i_{d,f} = 0$ and $i_{q,f} = 2\pi f_n C_f V_g$, where V_g is the peak value of phase voltage;
- Then, at the time $t = 0.5$ seconds, a step is applied in the direct current reference to 0.7 pu;
- Finally, at the time $t = 0.55$ seconds, a step is applied in quadrature current reference to 0.7 pu. Under these conditions, the grid current reaches approximately 1 pu.

Fig. 18 presents the obtained results for the converter current feedback strategy. As observed in Fig. 18 (a) – (c), PD, CCF and CVF strategies present similar behavior. This fact is justified by the design, which considered the same damping factor for all strategies. On the other hand, the NF strategy presents a larger overshoot. This is explained by the grid inductance, which changes the resonance frequency and decreases the effectiveness of the notch filter. Fig. 18 (e) shows that the capacitor voltage feedback provides the best result in terms of harmonic mitigation, since this technique provides a harmonic reduction at both resonance frequency and low frequency range.

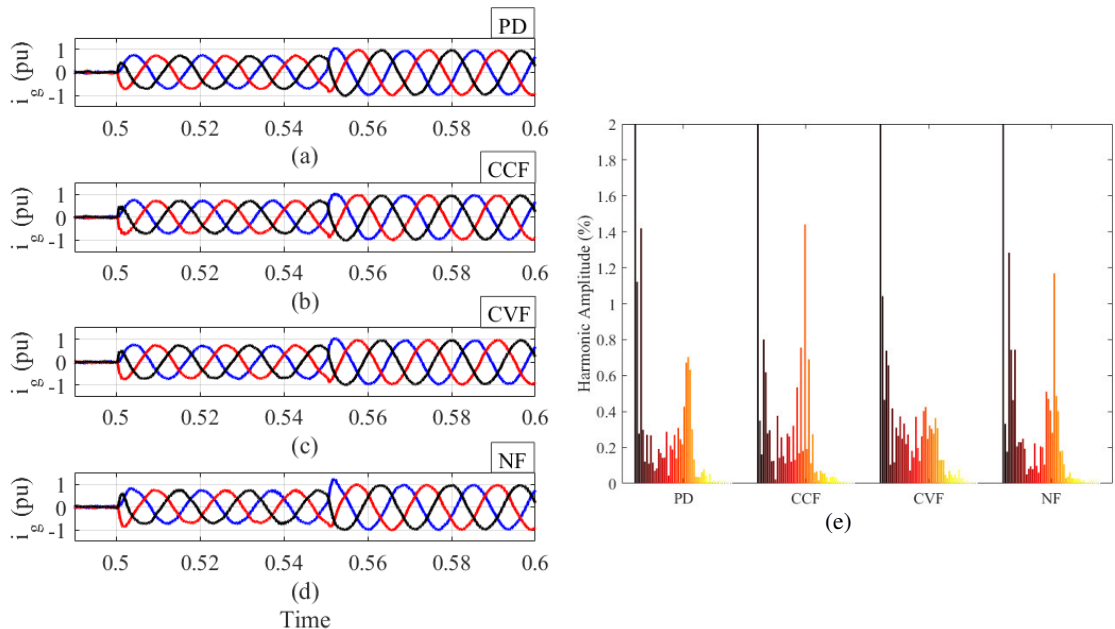


Fig. 18. Dynamic behavior of grid current when converter current feedback is employed for: (a) PD strategy (b) CCF strategy; (c) CVF strategy; (d) NF strategy. (e) Harmonic spectra for each damping strategy after $t = 0.56$ seconds.

Fig. 19 presents the results obtained for grid current feedback. As observed in Fig. 19 (a) – (d), both strategies present a similar behavior. The effectiveness of NF strategy is also decreased by grid inductance. However, for the design considered, the grid current control is inherently stable. Therefore, this effect is not evident. Fig. 19 (e) shows that the PD and the CVF strategies provide the best results for harmonic mitigation.

Table VI summarizes the results for total harmonic distortion of grid voltage and current. As observed, CVF strategy presents the lower THD for converter current feedback, for both grid voltage and current. Furthermore, CVF and PD present similar results for grid current feedback. It is important to note that THD considers only the harmonics until the 50th order (3 kHz). However, if this computation is extended to the 100th harmonic, PD presents the worst result for harmonic distortion, since the use of the passive damping resistor reduces filter attenuation.

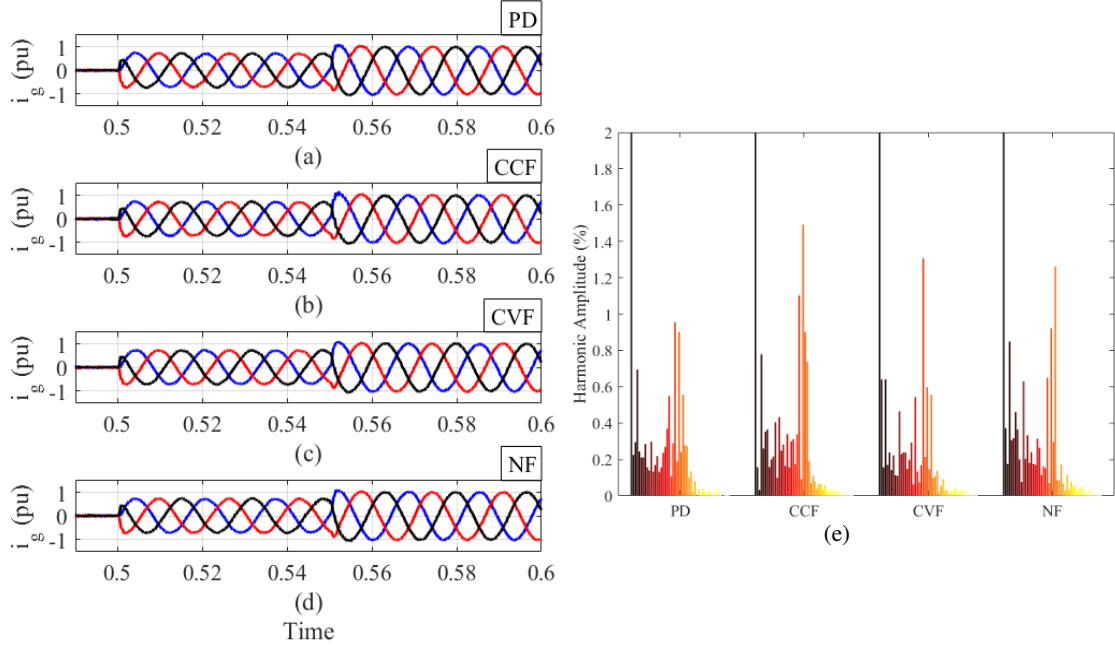


Fig. 19. Dynamic behavior of grid current when grid current feedback is employed for: (a) PD strategy (b) CCF strategy; (c) CVF strategy; (d) NF strategy. (e) Harmonic spectra for each damping strategy after $t = 0.56$ seconds.

Table VI. Total harmonic distortion for each damping strategy.

Feedback Strategy	THD (%)	PD	CCF	CVF	NF
i_f	i_g	2.54	2.48	2.20	2.60
	v_g	1.06	1.30	0.82	1.19
i_g	i_g	2.01	2.62	2.09	2.31
	v_g	1.12	1.54	1.09	1.28

6. Harmonic rejection performance

The study of the harmonic rejection capability is an important issue under weak grid conditions, since distorted voltages can appear in the PCC. According to [53], the effect of harmonic voltages in the inverter current control can be analyzed by means of impedance models. In this context, this reference proposes a Norton equivalent circuit for the grid connected inverter, which is interesting for aggregation studies.

An alternative approach is to determine the transfer function $H_R(s)$, given by [38]:

$$H_R(s) = \left. \frac{I_g(s)}{V_g(s)} \right|_{i^*=0}. \quad (68)$$

This transfer function can be easily determined by means of block diagrams. Using the block diagrams of Fig. 7, the harmonic rejection can be analyzed for the passive damping by means of:

$$H_{R,PD}^f(s) = \frac{-sC_f[sL_f + R_f + G_d(s)G_c(s)] + Z_d(s)(G_d(s) - 1)}{G_f(s) + [Z_d(s) - 1](sL_T + R_T) + G_d(s)G_c(s)[sC_f(sL_g + R_g)]}, \quad (69)$$

$$H_{R,PD}^g(s) = \frac{-sC_f(sL_f + R_f) + Z_d(s)(G_d(s) - 1)}{G_f + [Z_d(s) - 1][sL_T + R_T] + G_d(s)G_c(s)Z_d(s)}, \quad (70)$$

where $G_f(s) = s^3C_fL_fL_g + s^2C_f(L_fR_g + L_gR_f) + s(L_f + L_g + C_fR_F R_g) + R_f + R_g$ and $Z_d(s) = 1 + sC_fR_d$.

On the other hand, from Fig. 10, it is possible to obtain the equation below for capacitor current feedback:

$$H_{R,CCF}^f(s) = \frac{-sC_f[(sL_f + R_f) + G_d(s)[G_c(s) + K_c]] + G_d(s) - 1}{G_f + G_d(s)[sC_f(sL_g + R_g)(G_c(s) - K_c) + sC_fG_c(s)]}, \quad (71)$$

$$H_{R,CCF}^g(s) = \frac{-sC_f(sL_f + R_f) + sC_fK_cG_d(s) + G_d(s) - 1}{G_f + G_d(s)[G_c(s) + sC_fK_c(sL_g + R_g)]}. \quad (72)$$

Additionally, for capacitor voltage feedback, it is possible to obtain from Fig. 12 that:

$$H_{R,CVF}^f(s) = \frac{-sC_f[(sL_f + R_f) + G_d(s)[G_c(s) + L(s)]] + G_d(s) - 1}{G_f(s) + G_d(s)[G_c(s)C_f(sL_g + R_g) + 1] - L(s)(sL_g + R_g)], \quad (73)$$

$$H_{R,CVF}^g(s) = \frac{-sC_f(sL_f + R_f) + G_d(s)L(s) + G_d(s) - 1}{G_f(s) + G_d(s)[G_c(s) - L(s)(sL_g + R_g)]}. \quad (74)$$

Finally, by means of Fig. 15, it is possible to obtain for notch filter that:

$$H_{R,NF}^f(s) = \frac{-sC_f(sL_f + R_f + G_c(s)G_d(s)N(s)) + G_d(s) - 1}{G_f(s) + G_d(s)[G_c(s)N(s)[sC_f(sL_g + R_g) + 1]]}, \quad (75)$$

$$H_{R,NF}^g(s) = \frac{-sC_f(sL_f + R_f) + G_d(s) - 1}{G_f(s) + G_d(s)G_c(s)N(s)}. \quad (76)$$

The Bode diagrams of these transfer functions are presented in Fig. 20 (a) and (b) for grid and converter current feedback, respectively. As observed, the NF based strategy presents the worst behavior for harmonic rejection, due to its visible resonances.

Additionally, for converter current feedback, a larger impedance is observed at the range of 300 – 600 Hz, which contains the most common harmonics in power systems. Thereby, for the 5th and 7th harmonic orders, the converter current feedback is more susceptible than the grid current feedback strategy.

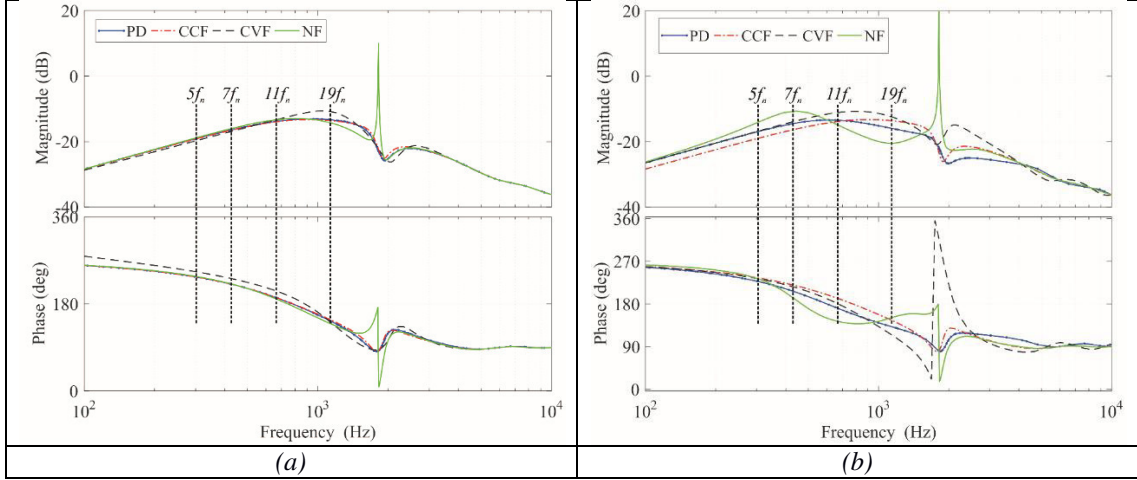


Fig. 20. Harmonic rejection transfer function of the studied damping structures for: (a) Grid current feedback strategies; (b) Converter current feedback strategies.

In order to verify the impedance characteristic of Fig. 20, the experimental voltage profile presented in Fig. 21 (a), is loaded in the simulation model. This voltage profile presents a noticeable 5th harmonic component, as shown in Fig. 21 (b). The harmonic spectra of Fig. 22 are obtained using this voltage profile. The effect of harmonic voltages can be reduced if other control strategies were employed. Literature suggests the use of resonant or repetitive controllers tuned in the harmonic frequency in order to improve the robustness of the inverter towards harmonic voltages [53,79,80]. It is important to note that, in this case study, no strategy to reduce the effect of harmonic voltages was explored.

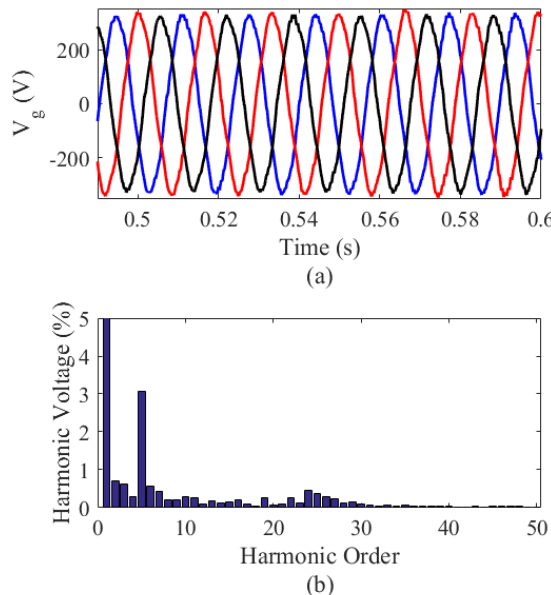


Fig. 21. Experimental voltage profile used in the harmonic rejection study: (a) Three-phase voltages in time domain; (b) Harmonic spectrum of phase A voltage.

As observed in Fig. 22, the current harmonic spectra is correlated with the harmonic rejection transfer function, which demonstrates that the notch filter strategy presents the largest 5th harmonic component for both converter and grid current feedback strategies. Furthermore, converter current feedback strategies present 5th harmonic component larger than that of the grid current feedback strategies, as aforementioned. Finally, the amplitudes for 5th harmonic are similar for grid current feedback strategy, since the harmonic rejection transfer function of all strategies has similar gain at this frequency.

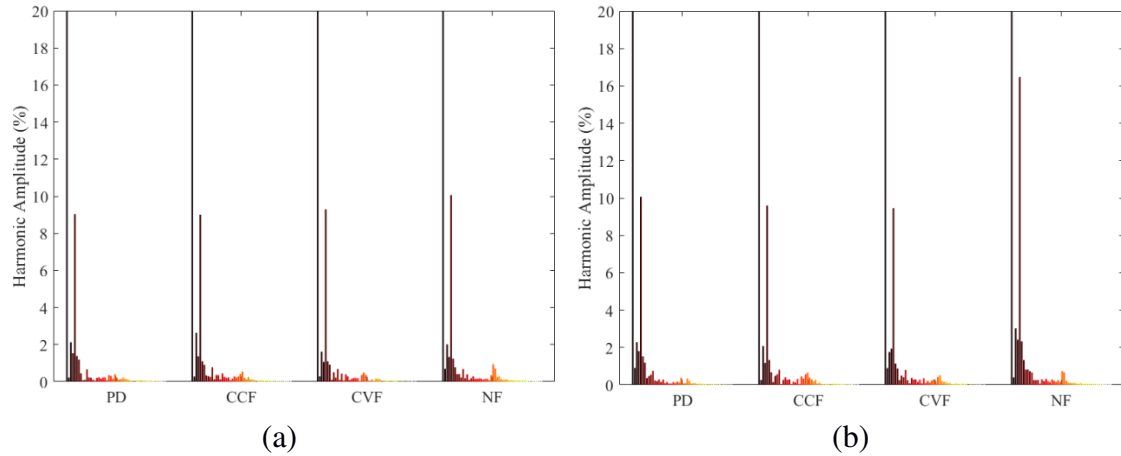


Fig. 22. Harmonic spectra for each damping strategy for the experimental voltage profile: (a) Grid current feedback strategies (b) Converter current feedback strategies.

7. Conclusions

This work presented a detailed review on four strategies for damping in a grid-connected three-phase PV system based on LCL filter. An analysis on low frequency models and control design was presented. Discussions about grid current and converter current feedback were also provided. The design methodology based on root locus in z-plane was employed and satisfactory responses were obtained for all strategies.

Additionally, the transfer functions of the harmonic rejection capability of each damping strategy are illustrated. A case study of a 10 kW inverter is used to evaluate the control dynamic response and the harmonic rejection capability. Different performances were observed for each damping strategy in the presence of grid voltage harmonics.

Finally, the comparison of each strategy can be summarized in Table VII.

Table VII. Comparison of the damping strategies approached in this work.

Damping Strategy	Advantages	Drawbacks
SPD	<ul style="list-style-type: none"> • Simplicity; • No need for modification in the control algorithm ; • Simpler control design; • No additional measurements; • Small effect in the low frequency poles. • Robust performance towards grid voltage harmonic distortion. 	<ul style="list-style-type: none"> • Increased converter power losses; • Heating in the damping resistor; • Increased filter volume; • Reduced attenuation in high frequencies; • Larger harmonic distortion, mainly due to high frequency components; • Poor performance towards weak grid conditions.
CCF	<ul style="list-style-type: none"> • No increase in power losses; • Similar effect in the transfer function, if compared with passive damping; • Robust performance towards grid voltage harmonic distortion; • Robust performance towards weak grid conditions. 	<ul style="list-style-type: none"> • Additional current measurement at the capacitor branch; • Cost of the current sensors; • Effect on the low frequency dynamic behavior – can lead to instability; • Noise in the capacitor current can affect control performance; • Poor performance in terms of current harmonic mitigation.
CVF	<ul style="list-style-type: none"> • No increase in power losses; • Good performance for current harmonic mitigation; • Robust performance towards weak grid conditions; • Robust performance towards grid voltage harmonic distortion. 	<ul style="list-style-type: none"> • Additional voltage measurement at the capacitor branch; • Cost of the voltage sensors; • Effect on the low frequency dynamic behavior – can lead to instability; • Noise in the capacitor voltage can affect control performance; • Implementation of lead-lag network increases the computational effort.
NF	<ul style="list-style-type: none"> • No increase in power losses; • Good performance towards grid harmonic distortion; • No need for modifications in the control algorithm; • No additional measurements. 	<ul style="list-style-type: none"> • Effect on the low frequency dynamic behavior – can lead to instability; • Implementation of notch increases the computational effort, mainly when a high number of sections is used; • Poor performance towards weak grid conditions.

8. Acknowledgments

The authors would like to thank the Brazilian agencies FAPEMIG, CNPq and CAPES by funding.

9. References

- [1] F. Blaabjerg, R. Teodorescu, M. Liserre, A. V. Timbus, Overview of control and grid synchronization for distributed power generation systems, *IEEE Trans. Ind. Electron.* 53 (2006) 1398–1409. doi:10.1109/TIE.2006.881997.
- [2] P. Chiradeja, R. Ramakumar, An approach to quantify the technical benefits of distributed generation, *IEEE Trans. Energy Convers.* 19 (2004) 764–773. doi:10.1109/TEC.2004.827704.
- [3] I.J. Gabe, V.F. Montagner, H. Pinheiro, Design and implementation of a robust current controller for VSI connected to the grid through an LCL filter, *IEEE Trans.*

- Power Electron. 24 (2009) 1444–1452. doi:10.1109/TPEL.2009.2016097.
- [4] M. Liserre, A. Dell’Aquila, F. Blaabjerg, Stability improvements of an LCL-filter based three-phase active rectifier, in: 2002 IEEE 33rd Annu. IEEE Power Electron. Spec. Conf., 2002: pp. 1195–1201. doi:10.1109/PSEC.2002.1022338.
- [5] M. Büyük, A. Tan, M. Tümay, K.Ç. Bayındır, Topologies, generalized designs, passive and active damping methods of switching ripple filters for voltage source inverter: A comprehensive review, Renew. Sustain. Energy Rev. 62 (2016) 46–69. doi:10.1016/j.rser.2016.04.006.
- [6] IEEE Std 519-1992, IEEE recommended practices and requirements for harmonic control in electrical power systems, 1992.
- [7] IEC Standard 61000-3-6, Assessment of emission limits for distorting loads in MV and HV power systems, 2008.
- [8] V. Ponnaluri, V. Krishnamurthy, V. Kanetkar, Generalized system design and analysis of PWM based power electronic converters, in: Proc. Ind. Appl. Conf., 2000: pp. 1972–1979.
- [9] V. Blasko, V. Kaura, A novel control to actively damp resonance in input LC filter of a three-phase voltage source converter, IEEE Trans. Ind. Appl. 33 (1997) 542–550. doi:10.1109/28.568021.
- [10] Y.W. Li, Control and resonance damping of voltage-source and current-source converters with LC filters, IEEE Trans. Ind. Electron. 56 (2009) 1511–1521. doi:10.1109/TIE.2008.2009562.
- [11] H. Kim, S.K. Sul, A novel filter design for output LC filters of PWM inverters, J. Power Electron. 11 (2011) 74–81. doi:10.1109/IPEMC.2009.5157417.
- [12] J. He, Y.W. Li, Generalized closed-loop control schemes with embedded virtual impedances for voltage source converters with LC or LCL filters, IEEE Trans. Power Electron. 27 (2012) 1850–1861. doi:10.1109/TPEL.2011.2168427.
- [13] A. Houari, H. Renaudineau, J.P. Martin, S. Pierfederici, F. Meibody-Tabar, Flatness-based control of three-phase inverter with output LC filter, IEEE Trans. Ind. Electron. 59 (2012) 2890–2897. doi:10.1109/TIE.2011.2170396.
- [14] R. Pena-Alzola, M. Liserre, F. Blaabjerg, M. Ordóñez, Y. Yang, LCL-filter design for robust active damping in grid-connected converters, IEEE Trans. Ind. Informatics. 10 (2014) 2192–2203. doi:10.1109/TII.2014.2361604.
- [15] R. Pena-Alzola, M. Liserre, F. Blaabjerg, R. Sebastian, J. Dannehl, F.W. Fuchs, Systematic Design of the Lead-Lag Network Method for Active Damping in LCL-Filter Based Three Phase Converters, Ind. Informatics, IEEE Trans. 10 (2014) 43–52. doi:10.1109/TII.2013.2263506.
- [16] R. Pe, M. Liserre, F. Blaabjerg, T. Kerekes, Self-commissioning Notch Filter for Active Damping in Three Phase LCL -filter Based Grid-tie Converter, IEEE Trans. Power Electron. 8993 (2014) 1–9. doi:10.1109/TPEL.2014.2304468.
- [17] R. Pena-Alzola, M. Liserre, F. Blaabjerg, R. Sebastian, J. Dannehl, F.W. Fuchs, Analysis of the passive damping losses in lcl-filter-based grid converters, IEEE Trans. Power Electron. 28 (2013) 2642–2646. doi:10.1109/TPEL.2012.2222931.
- [18] W. Wu, Y. Sun, M. Huang, X. Wang, H. Wang, F. Blaabjerg, M. Liserre, H.S.H. Chung, A robust passive damping method for LLCL-filter-based grid-tied inverters to minimize the effect of grid harmonic voltages, IEEE Trans. Power Electron. 29 (2014) 3279–3289. doi:10.1109/TPEL.2013.2279191.
- [19] W. Wu, Y. He, F. Blaabjerg, An LLCL power filter for single-phase grid-tied inverter, IEEE Trans. Power Electron. 27 (2012) 782–789. doi:10.1109/TPEL.2011.2161337.
- [20] W. Wu, Y. He, T. Tang, F. Blaabjerg, A new design method for the passive damped

- LCL and LLCL filter-based single-phase grid-tied inverter, *IEEE Trans. Ind. Electron.* 60 (2013) 4339–4350. doi:10.1109/TIE.2012.2217725.
- [21] J. Xu, J. Yang, J. Ye, Z. Zhang, A. Shen, An LCL filter for three-phase grid-connected converters, *IEEE Trans. Power Electron.* 29 (2014) 4322–4338. doi:10.1109/TPEL.2013.2292000.
 - [22] A.A. Rockhill, M. Liserre, R. Teodorescu, P. Rodriguez, Grid Filter Design for a Multi-Megawatt Medium-Voltage Voltage Source Inverter, *IEEE Trans. Ind. Electron.* 58 (2011) 1205–1217. doi:10.1109/TIE.2010.2087293.
 - [23] H. Cha, T.K. Vu, Comparative analysis of low-pass output filter for single-phase grid-connected photovoltaic inverter, in: *IEEE Appl. Power Electron. Conf. Expo.*, 2010: pp. 1659–1665. doi:10.1109/APEC.2010.5433454.
 - [24] J. Dannehl, M. Liserre, F.W. Fuchs, Filter-based active damping of voltage source converters with LCL filter, *IEEE Trans. Ind. Electron.* 58 (2011) 3623–3633. doi:10.1109/TIE.2010.2081952.
 - [25] Y. Tang, P.C. Loh, P. Wang, F.H. Choo, F. Gao, F. Blaabjerg, Generalized design of high performance shunt active power filter with output LCL filter, *IEEE Trans. Ind. Electron.* 59 (2012) 1443–1452. doi:10.1109/TIE.2011.2167117.
 - [26] R.N. Beres, X. Wang, F. Blaabjerg, M. Liserre, C.L. Bak, Optimal Design of High-Order Passive-Damped Filters for Grid-Connected Applications, *IEEE Trans. Power Electron.* 31 (2016) 2083–2098.
 - [27] M. Zabaleta, E. Burguete, D. Madariaga, I. Zubimendi, M. Zubia, I. Larrazabal, LCL Grid Filter Design of a Multimegawatt Medium-Voltage Converter for Offshore Wind Turbine Using SHEPWM Modulation, *IEEE Trans. Power Electron.* 31 (2016) 1993–2001.
 - [28] M. Liserre, F. Blaabjerg, A. Dell'Aquila, Step-by-step design procedure for a grid-connected three-phase PWM voltage source converter, *Int. J. Electron.* 91 (2004) 445–460. doi:10.1080/00207210412331306186.
 - [29] J. Dannehl, C. Wessels, F.W. Fuchs, Limitations of voltage - oriented PI current control of grid - connected PWM rectifiers with LCL filters, *IEEE Trans. Ind. Electron.* 56 (2009) 380–388. doi:10.1109/TIE.2008.2008774.
 - [30] C. Zhang, T. Dragicevic, J.C. Vasquez, J.M. Guerrero, Resonance damping techniques for grid-connected voltage source converters with LCL filters - A review, in: *IEEE Int. Energy Conf.*, 2014: pp. 169–176. doi:10.1109/ENERGYCON.2014.6850424.
 - [31] J. Yin, S. Duan, B. Liu, Stability analysis of grid-connected inverter with LCL filter adopting a digital single-loop controller with inherent damping characteristic, *IEEE Trans. Ind. Informatics.* 9 (2013) 1104–1112. doi:10.1109/TII.2012.2222424.
 - [32] J. Dannehl, F.W. Fuchs, S. Hansen, P.B. Thogersen, Investigation of active damping approaches for PI-based current control of grid-connected pulse width modulation converters with LCL filters, *IEEE Trans. Ind. Appl.* 46 (2010) 1509–1517. doi:10.1109/TIA.2010.2049974.
 - [33] R. Beres, X. Wang, F. Blaabjerg, C.L. Bak, M. Liserre, A review of passive filters for grid-connected voltage source converters, in: *IEEE Appl. Power Electron. Conf. Expo.*, 2014: pp. 2208–2215. doi:10.1109/APEC.2014.6803611.
 - [34] R. Teodorescu, M. Liserre, P. Rodriguez, *Grid Converters for Photovoltaic and Wind Power Systems*, Willey, 2011.
 - [35] W. Gullvik, L. Norum, R. Nilsen, Active damping of resonance oscillations in LCL-filters based on virtual flux and virtual resistor, in: *Eur. Conf. Power Electron. Appl.*, 2007. doi:10.1109/EPE.2007.4417734.

- [36] W.Y. Yang, W. Cao, T.S. Chung, J. Morris, A simple voltage sensorless active damping scheme for three-phase PWM converters with an LCL filter, *IEEE Trans. Ind. Electron.* 55 (2005) 1876–1880. doi:10.1109/TIE.2008.917066.
- [37] Guoqiao Shen, Dehong Xu, Luping Cao, Xuancai Zhu, An Improved Control Strategy for Grid-Connected Voltage Source Inverters With an LCL Filter, *IEEE Trans. Power Electron.* 23 (2008) 1899–1906. doi:10.1109/TPEL.2008.924602.
- [38] J. Xu, S. Xie, T. Tang, Active Damping-Based Control for Grid-Connected LCL-Filtered Inverter With Injected Grid Current Feedback Only, *IEEE Trans. Ind. Electron.* 61 (2014) 4746–4758. doi:10.1109/TIE.2013.2290771.
- [39] X. Wang, F. Blaabjerg, P.C. Loh, Grid-Current-Feedback Active Damping for LCL Resonance in Grid-Connected Voltage-Source Converters, *IEEE Trans. Power Electron.* 31 (2016) 213–223.
- [40] E. Twining, D.G. Holmes, Grid current regulation of a three-phase voltage source inverter with an LCL input filter, *IEEE Trans. Power Electron.* 18 (2003) 888–895. doi:10.1109/TPEL.2003.810838.
- [41] C. Bao, X. Ruan, X. Wang, W. Li, D. Pan, K. Weng, Step-by-step controller design for LCL-Type Grid-Connected inverter with capacitor-current-feedback active-damping, *IEEE Trans. Power Electron.* 29 (2014) 1239–1253. doi:10.1109/TPEL.2013.2262378.
- [42] N. He, D. Xu, Y. Zhu, J. Zhang, G. Shen, Y. Zhang, J. Ma, C. Liu, Weighted average current control in a three-phase grid inverter with an LCL filter, *IEEE Trans. Power Electron.* 28 (2013) 2785–2797. doi:10.1109/TPEL.2012.2219322.
- [43] G. Shen, X. Zhu, J. Zhang, D. Xu, A new feedback method for PR current control of LCL-filter-based grid-connected inverter, *IEEE Trans. Ind. Electron.* 57 (2010) 2033–2041. doi:10.1109/TIE.2010.2040552.
- [44] S. Mariéthoz, M. Morari, Explicit model-predictive control of a PWM inverter with an LCL filter, *IEEE Trans. Ind. Electron.* 56 (2009) 389–399. doi:10.1109/TIE.2008.2008793.
- [45] J.R. Massing, H. Pinheiro, Adaptive current control of grid-connected VSC with LCL-filters using parallel feedforward compensation, in: *Ind. Electron. Conf.*, 2010: pp. 3185–3191. doi:10.1109/IECON.2010.5675046.
- [46] B. Bahrani, M. Vasiladiotis, A. Rufer, High-order vector control of grid-connected voltage-source converters with LCL-filters, *IEEE Trans. Ind. Electron.* 61 (2014) 2767–2775. doi:10.1109/TIE.2013.2276442.
- [47] Y. Lei, Z. Zhao, F. He, S. Lu, L. Yin, An improved virtual resistance damping method for grid-connected inverters with LCL filters, in: *IEEE Energy Convers. Congr. Expo. Energy Convers. Innov. a Clean Energy Futur.*, 2011: pp. 3816–3822. doi:10.1109/ECCE.2011.6064287.
- [48] R. Teodorescu, F. Blaabjerg, M. Liserre, A. Dell'Aquila, A stable three-phase LCL-filter based active rectifier without damping, in: *IAS Annu. Meet. Conf. Rec. Ind. Appl. Conf.*, 2003: pp. 1552–1557. doi:10.1109/IAS.2003.1257762.
- [49] J.L. Agorreta, M. Borrega, J. López, L. Marroyo, Modeling and control of N-paralleled grid-connected inverters with LCL filter coupled due to grid impedance in PV plants, *IEEE Trans. Power Electron.* 26 (2011) 770–785. doi:10.1109/TPEL.2010.2095429.
- [50] M. Liserre, R. Teodorescu, F. Blaabjerg, Stability of photovoltaic and wind turbine grid-connected inverters for a large set of grid impedance values, *IEEE Trans. Power Electron.* 21 (2006) 263–271. doi:10.1109/TPEL.2005.861185.
- [51] C. Yu, X. Zhang, F. Liu, F. Li, H. Xu, R. Cao, H. Ni, Modeling and Resonance Analysis of Multiparallel Inverters System Under Asynchronous, *IEEE Trans.*

- Power Electron. 32 (2017) 3192–3205.
- [52] M. Lu, X. Wang, P.C. Loh, F. Blaabjerg, Resonance Interaction of Multiparallel Grid-Connected Inverters With LCL Filter, *IEEE Trans. Power Electron.* 32 (2017) 894–899.
- [53] F. Wang, J.L. Duarte, M.A.M. Hendrix, P.F. Ribeiro, Modeling and analysis of grid harmonic distortion impact of aggregated DG inverters, *IEEE Trans. Power Electron.* 26 (2011) 786–797. doi:10.1109/TPEL.2010.2091286.
- [54] M. Liserre, F. Blaabjerg, S. Hansen, Design and control of an LCL-filter-based three-phase active rectifier, *IEEE Trans. Ind. Appl.* 41 (2005) 1281–1291. doi:10.1109/TIA.2005.853373.
- [55] J. Muhlethaler, S. Mario, R. Blattmann, J.W. Kolar, A. Ecklebe, Optimal Design of LCL Harmonic Filters for Three-Phase PFC Rectifiers, 28 (2011) 3114–3125.
- [56] K. Jalili, S. Bernet, Design of LCL filters of active-front-end two-level voltage-source converters, *IEEE Trans. Ind. Electron.* 56 (2009) 1674–1689. doi:10.1109/TIE.2008.2011251.
- [57] A. Reznik, M.G. Simoes, A. Al-Durra, S.M. Muyeen, LCL Filter design and performance analysis for grid-interconnected systems, *IEEE Trans. Ind. Appl.* 50 (2014) 1225–1232. doi:10.1109/TIA.2013.2274612.
- [58] P. Channegowda, V. John, Filter Optimization for Grid Interactive Voltage Source Inverters, *IEEE Trans. Ind. Electron.* 57 (2010) 4106–4114. doi:10.1109/TIE.2010.2042421.
- [59] N. Kroutikova, C.A. Hernandez-Aramburo, T.C. Green, State-space model of grid-connected inverters under current control mode, *IET Eletr. Power Appl.* 1 (2007) 329–338. doi:10.1049/iet-epa.
- [60] Y. Tang, W. Yao, P.C. Loh, F. Blaabjerg, Design of LCL Filters With LCL Resonance Frequencies Beyond the Nyquist Frequency for Grid-Connected Converters, *IEEE J. Emerg. Ans Sel. Top. Power Electron.* 4 (2016) 3–14.
- [61] S. Jayalath, M. Hanif, Generalized LCL-Filter Design Algorithm for Grid-Connected Voltage-Source Inverter, *IEEE Trans. Ind. Electron.* 64 (2017) 1905–1915.
- [62] M.P. Kazmierkowski, L. Malesani, Current Control Techniques for Three-Phase Voltage-Source PWM Converters : A Survey, *IEEE Trans. Ind. Electron.* 45 (1998) 691–703.
- [63] R. Razi, M. Monfared, Simple control scheme for single-phase uninterruptible power supply inverters with Kalman filter-based estimation of the output voltage, *IET Power Electron.* 8 (2005) 1817–1824. doi:10.1049/iet-pel.2014.0929.
- [64] W.Y. Yang, W. Cao, T.S. Chung, J. Morris, Observer-Based State-Space Current Controller for a Grid Converter Equipped With an LCL Filter : Analytical Method for Direct Discrete-Time Design, *IEEE Trans. Ind. Appl.* 51 (2005) 4079–4090.
- [65] H. Komurcugil, S. Member, S. Ozdemir, I. Sefa, Sliding-Mode Control for Single-Phase Grid-Connected LCL-Filtered VSI With Double-Band Hysteresis Scheme, *IEEE Trans. Ind. Electron.* 63 (2016) 864–873.
- [66] V.S.I. With, X. Hao, S. Member, X. Yang, T. Liu, L. Huang, W. Chen, A Sliding-Mode Controller With Multiresonant Sliding Surface for Single-Phase Grid-Connected, *IEEE Trans. Power Electron.* 28 (2013) 2259–2268.
- [67] L. Harnefors, L. Zhang, M. Bongiorno, Frequency-domain passivity-based current controller design, *IET Power Electron.* 1 (2008) 455–465. doi:10.1049/iet-pel.
- [68] M. Bottcher, J. Dannehl, F.W. Fuchs, Interconnection and Damping Assignment Passivity-Based Current Control of Grid-Connected PWM Converter with, in: 14th Int. Power Electron. Motion Control Conf., 2010: pp. 20–26.

- [69] L. Harnefors, A.G. Yépes, A. Vidal, J. Doval-gandoy, Passivity-Based Controller Design of Grid-Connected VSCs for Prevention of Electrical Resonance Instability, *IEEE Trans. Ind. Electron.* 62 (2015) 702–710.
- [70] T. Liu, X. Hao, X. Yang, M. Zhao, Q. Huang, L. Huang, A Novel Repetitive Control Scheme For Three-phase Grid-connected Inverter with LCL Filter, in: 2012 IEEE 7th Int. Power Electron. Motion Control Conf., 2012: pp. 335–339.
- [71] J. Xu, S. Xie, T. Tang, Evaluations of current control in weak grid case for grid-connected LCL-filtered inverter, *IET Power Electron.* (2013) 227–234. doi:10.1049/iet-pel.2012.0192.
- [72] G.I. With, O. Lcl, Z. Zou, S. Member, Z. Wang, M. Cheng, S. Member, Modeling , Analysis , and Design of Multifunction, *IEEE Trans. Power Electron.* 29 (2014) 3830–3839.
- [73] M. Jasinski, M. Liserre, F. Blaabjerg, M. Cichowlas, Fuzzy Logic Current Controller for PWM Rectifiers, in: *Ind. Electron. Conf.*, 2002: pp. 1300–1305.
- [74] M. Rosyadi, S.M. Muyeen, R. Takahashi, J. Tamura, Fuzzy Logic Controlled Voltage Source Converter in Grid Connected Application via LCL Filter, in: 15th Int. Conf. Electr. Mach. Syst., 2012.
- [75] N. Thao, K. Uchida, Control The Photovoltaic Grid-Connected System Using Fuzzy Logic and Backstepping Approach, in: 9th Asian Control Conf., 2013.
- [76] W.Y. Yang, W. Cao, T.S. Chung, J. Morris, Robust Line-Voltage Sensorless Control and Synchronization of LCL -Filtered Distributed Generation Inverters for High Power Quality Grid Connection, *IEEE Trans. Power Electron.* 27 (2005) 87–98.
- [77] Y. He, H. Chung, C. Ho, W. Wu, Use of Boundary Control With Second-Order Switching Surface to Reduce the System Order for Deadbeat Controller in Grid-Connected Inverter, *IEEE Trans. Power Electron.* 31 (2016) 2638–2653.
- [78] E. Wu, P.W. Lehn, Digital Current Control of a Voltage Source Converter With Active Damping of LCL Resonance, *IEEE Trans. Power Electron.* 21 (2006) 1364–1373.
- [79] A.G. Yépes, S. Member, F.D. Freijedo, Ó. López, J. Doval-gandoy, Analysis and Design of Resonant Current Controllers for Voltage-Source Converters by Means of Nyquist Diagrams and Sensitivity Function, *IEEE Trans. Ind. Electron.* 58 (2011) 5231–5250.
- [80] A.G. Yépes, S. Member, F.D. Freijedo, Effects of Discretization Methods on the Performance of Resonant Controllers, *IEEE Trans. Power Electron.* 25 (2010) 1692–1712.
- [81] P. Rodríguez, R. Teodorescu, I.C. Candela, A. V Timbus, M. Liserre, F. Blaabjerg, New Positive-sequence Voltage Detector for Grid Synchronization of Power Converters under Faulty Grid Conditions, in: *Power Electron. Spec. Conf. 2006. PESC '06. 37th IEEE*, 2006: pp. 1–7.
- [82] P. Rodríguez, J. Pou, J. Bergas, J.I. Candela, R.P. Burgos, D. Boroyevich, Decoupled Double Synchronous Reference Frame PLL for Power Converters Control, *IEEE Trans. Power Electron.* 22 (2007) 584–592.
- [83] R. Teodorescu, F. Blaabjerg, U. Borup, M. Liserre, A New Control Structure for Grid-Connected LCL PV Inverters with Zero Steady-State Error and Selective Harmonic Compensation, in: 19th Annu. IEEE Appl. Power Electron. Conf. Expo., 2004: pp. 580–586.
- [84] S.G. Parker, B.P. McGrath, D.G. Holmes, Regions of Active Damping Control for LCL Filters, *IEEE Trans. Ind. Appl.* 50 (2014) 424–432.
- [85] Y. Tang, C. Yoon, R. Zhu, F. Blaabjerg, Generalized Stability Regions of Current

- Control for LCL-Filtered Grid-Connected Converters without Passive or Active Damping, in: 2015 IEEE Energy Convers. Congr. Expo., 2015: pp. 2040–2047.
- [86] W. Yao, Y. Yang, X. Zhang, F. Blaabjerg, Design and Analysis of Robust Active Damping for LCL Filters using Digital Notch Filters, *IEEE Trans. Power Electron.* 8993 (2016) 1–15. doi:10.1109/TPEL.2016.2565598.
- [87] P. Mattavelli, F. Polo, F.D. Lago, S. Saggini, Analysis of Control-Delay Reduction for the Improvement of UPS Voltage-Loop Bandwidth, *IEEE Trans. Ind. Electron.* 55 (2008) 2903–2911.
- [88] W.Y. Yang, W. Cao, T.S. Chung, J. Morris, *Applied Numerical Methods Using Matlab*, 1st ed., Wiley-Inter-science, New Yourk, USA, 2005.
- [89] V. Blasko, V. Kaura, A New Mathematical Model and Control of a Three-Phase AC–DC Voltage Source Converter, *IEEE Trans. Power Electron.* 12 (1997) 116–123.
- [90] X. Guo, W. Wu, H. Gu, Modeling and simulation of direct output current control for LCL-interfaced grid-connected inverters with parallel passive damping, *Simul. Model. Pract. Theory.* 18 (2010) 946–956. doi:10.1016/j.simpat.2010.02.010.
- [91] T.C. Wang, Z. Ye, G. Sinha, X. Yuan, Output Filter Design for a Grid-interconnected Three-phase Inverter, in: 34th Annu. Power Electron. Spec. Conf., 2003: pp. 779–784.
- [92] A.K. Balasubramanian, V. John, Analysis and design of split-capacitor resistive-inductive passive damping for LCL filters in grid-connected inverters, *IET Power Electron.* 6 (2013) 1822–1832. doi:10.1049/iet-pel.2012.0679.
- [93] C. Liu, K. Dai, K. Duan, Y. Kang, Application of a C-Type Filter Based LCFL Output Filter to Shunt Active Power Filters, *J. Power Electron.* 13 (2013) 1058–1069.
- [94] F. Liu, Y. Zhou, S. Duan, J. Yin, B. Liu, F. Liu, Parameter design of a two-current-loop controller used in a grid-connected inverter system with LCL filter, *IEEE Trans. Ind. Electron.* 56 (2009) 4483–4491. doi:10.1109/TIE.2009.2021175.
- [95] M. Orellana, R. Grino, On the stability of discrete-time active damping methods for VSI converters with a LCL input filter, in: Proc. Ind. Electron. Conf., 2012: pp. 2378–2383. doi:10.1109/IECON.2012.6388871.
- [96] Z. Xin, P.C. Loh, X. Wang, F. Blaabjerg, Y. Tang, Highly Accurate Derivatives for LCL -Filtered Grid Converter With Capacitor Voltage Active Damping, *IEEE Trans. Power Electron.* 31 (2016) 3612–3625.
- [97] M. Ciobotaru, A. Ross, L. Bede, B. Karanayil, Adaptive Notch Filter Based Active Damping for Power Converters Using LCL Filters, in: 2016 IEEE 7th Int. Symp. Power Electron. Distrib. Gener. Syst., 2016: pp. 1–7.